10

Study on Dynamic Characteristics of Six-axis Wrist Force/torque Sensor

Ke-Jun Xu
Institute of Automation, Hefei University of Technology, Hefei 230009, PRC

1. Introduction

It is necessary to detect complex force and torque components of three-dimensional space in research and manufacture, therefore the multi-axis force and torque sensors are developed rapidly. For examples, the six-axis wrist force/torque sensor for robot assembling and automated polishing [1,2], the multi-component strain gauge balance for wind tunnel testing to determine loads on models [3], the multi-axis measuring force platform for biomedical research and development, and so on [4]. Now the dynamic performances of multi-axis force and torque sensors are demanded strictly because these sensors are used in robot operation, dynamic testing and process control. However, the dynamic performances of multi-axis force sensor are not satisfied with the needs of applications. First, due to the small damped ratio and low natural frequency of sensor, the dynamic response of sensor is slow, and the time to reach steady state is long. Secondly, there are dynamic couples among various directions of multi-axis force and torque sensor because the elastic body of sensor is an integer structure and the interaction of various directions can not be avoided completely. Thirdly, the multi-axis force sensor possesses the nonlinear dynamic characteristics under some conditions, which will affect the measurement accuracy. It is necessary to study and solve these key problems. Therefore, this chapter focuses on the six-axis wrist force sensor, and introduces the dynamic calibration experiments, dynamic modeling, dynamic compensation and dynamic decoupling. Finally, it presents some researches on the nonlinear dynamic characteristics of the six-axis wrist force sensor.

2. Dynamic calibration experiments

Generally speaking, there are three kinds of dynamic calibration methods, that is, the frequency response method, the impact response method and the step response method. As for the wrist force sensor, it is difficult to generate sine wave to make an excitation because the natural frequency of some channels may be larger than 800 Hz and there are six channels. Therefore we carried out the impulse response experiment and step response experiment.

In the impulse response experimental, the impact force was generated by a hammer. A piezoelectric sensor was installed in the hammer to reflect the impulse force. When the

Source: Sensors, Focus on Tactile, Force and Stress Sensors, Book edited by: Jose Gerardo Rocha and Senentxu Lanceros-Mendez, ISBN 978-953-7619-31-2, pp. 444, December 2008, I-Tech, Vienna, Austria

impact force was applied to the wrist force sensor, both the eight-channel output of the wrist force sensor and the piezoelectric sensor output was collected by a data acquisition equipment at the same time. It is difficult to control the striking point and angle of the hammer and the strength of the force in the experiments, and it is impossible to perform the torque calibration.

In order to test the dynamic performance of the wrist force sensor accurately and strictly, we carried out the dynamic calibration experiments based on the step response method. The wrist force sensor was mounted horizontally in the center of a dynamic calibration test bench designed by the Institute of Intelligent Machines, Chinese Academy of Sciences. A round steel plate was fixed on the sensor through screws. In the center of the plate a bar was installed vertically, and in the top end of the bar there was a hook, which could be used to hang weights through a string so as to apply the force and torque. At four sides of the plate, four short bars were also mounted symmetrically, and there was a groove in the top end of each short bar. At four sides of the bench four supports were fixed, and fixed pulleys were mounted on the supports. A string was winded through the fixed pulleys of the supports, the hook of the bar and the grooves of the short bars. A weight hung on one end of the string, and the other end of the string was connected with a one-dimensional force sensor. When the string was cut with scissors fast, the weight suddenly fell to the ground, which generated a negative step force or torque for the wrist force sensor. This force or torque was measured and transformed into electrical signals by the one-dimensional force sensor. Fig. 2-1 (a), (b) and (c) showed the calibrations in different directions.

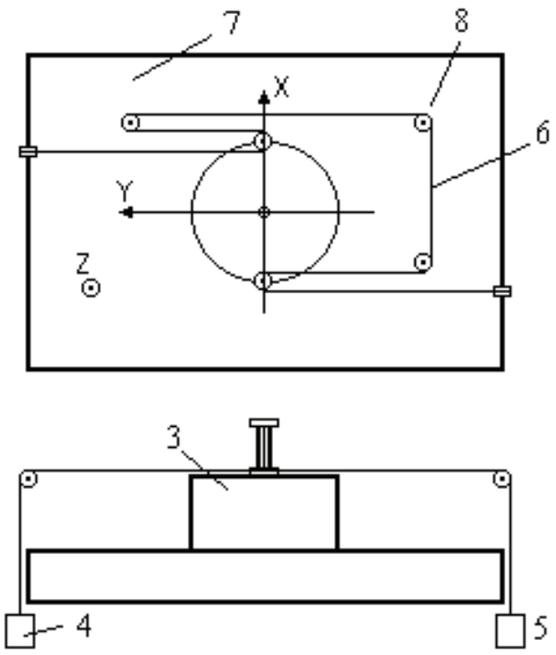

(a) Channel M_z

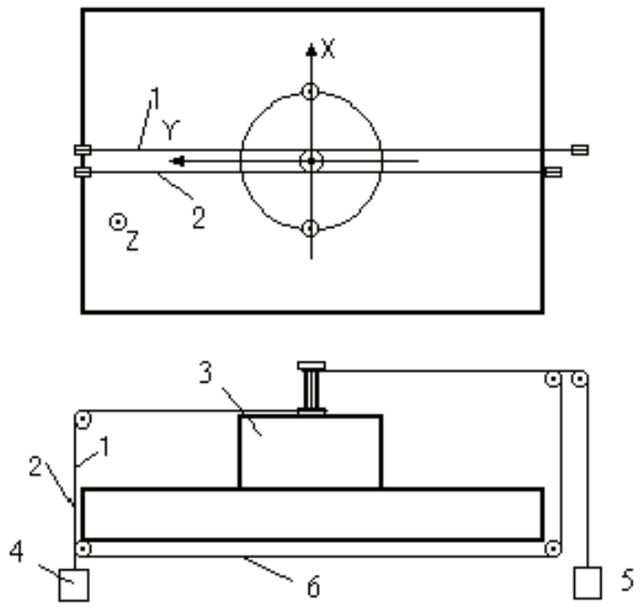

(b) Channel M_x

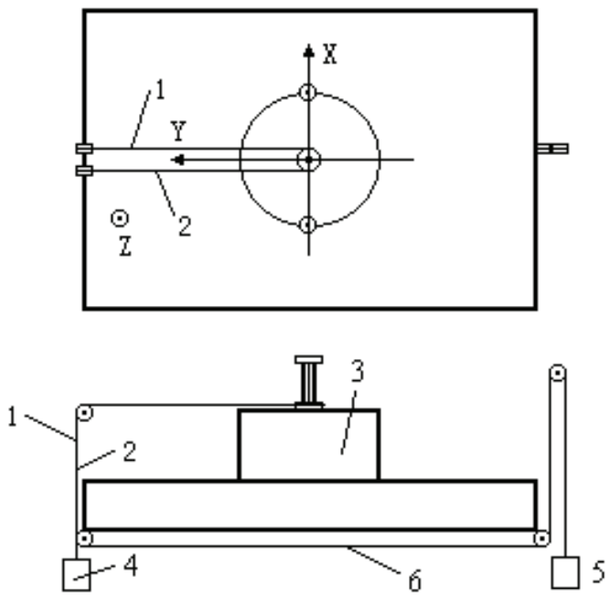

(c) Channel F_y

Fig. 2-1 Calibration schematic diagram (1) and (2) strip, (3) wrist force sensor, (4) one-dimensional force sensor, (5) weight, (6) cutting place, (7) calibration test table, (8) pulleys.

The elastic body of the wrist force sensor was a floating cross – beam, and shown in Fig. 2-2. Thirty-two pieces of strain gauges were adhered to the beam, forming eight electrical bridges. The outputs of the bridges were amplified and sent into the DSP-based real time dynamic compensation system developed by us. The signals of eight channels, which were acquired and decoupled by this system, are transformed into the signals of six channels, expressing F_x, F_y, F_z, M_x, M_y and M_z that were three force components and three torque components in the three dimensional space. At the same time, the system also conducted the dynamic compensation for the output signals of six channels so as to enhance the dynamic response of the wrist force sensor. The programs of real time data acquisition, decoupling and compensation are stored in an EPROM of the system. They could also be downloaded via the serial communication port by a PC. In the dynamic calibration, the exciting signal measured by a one–dimensional force sensor and the outputs of six channels of the wrist force sensor were collected by a MR30C recorder. At the same time, the exciting signal and the outputs of main channels of the wrist force sensor were captured by a COM7101A digital oscilloscope, and then stored in HP PC via a GP-IB bus.

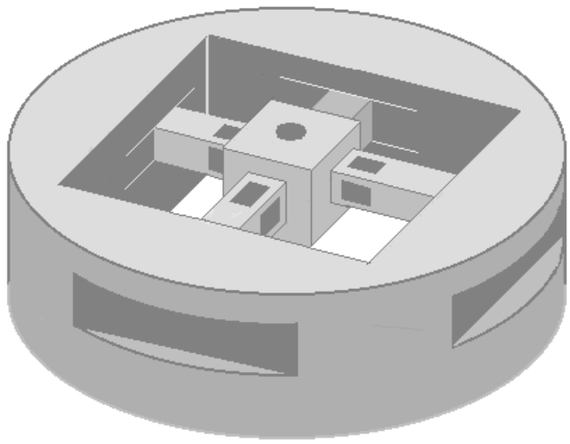

Fig. 2-2 Structure of elastic body

The calibration procedure was as follows.

1. Adjusting the zero point of the amplifiers of the wrist force sensor.
2. Applying the force or torque to the wrist force sensor through hanging weights, and measuring the static output voltages of eight channels of the wrist force sensor and one of six channels of the dynamic correcting system.
3. Cutting the string on which the weights were hung, and generating the step form excitation force or torque. Then measuring and recording the dynamic exciting signal and response signals of the wrist force sensor. The work of measuring and recording was done three times for each channel of the wrist force sensor.

3. Dynamic modeling

In order to describe accurately the dynamic characteristics of the wrist force sensor, its dynamic models are built with various methods, such as the system identification, the Walsh transformation, the time series analysis and the artificial neural network according to the step response experimental data.

3.1 Preprocessing

Before modeling, the experimental data must be pretreated.

1) Construction of exciting signal

In the dynamic calibration experiments, not suitable one-dimensional force sensor (that is to say, the sensor has no ideal frequency characteristic) could be used to test the practical step-form exciting signal, i.e. the release process of the weight. Although the string was cut off fast, the weight suddenly released, which was equal to the negative step force theoretically. In the actual situation, however, the string was elastic and goes through the pulleys, so the string was subjected to the frictional force and its speed of release slowed down. Therefore, the step signal was not an ideal step wave. If the step wave was regarded as the exciting signal, it was not satisfied with the actual conditions, and the results of modeling were poor. So we have to construct the exciting signal according to the step response because the step response of the wrist force sensor is caused by the exciting signal.

a. It is supposed that the sensor is a two-order system.
b. The starting points of both the exciting signal and step response are the same.
c. In many cases, the amplitude of the exciting signal is equal to the steady status value of the step response.
d. The rising part of the exciting signal is constructed so as to make the difference between the step response and the exciting signal be an attenuated oscillation curve.

2) Data filtered

In the measurement and transforming processes of dynamic signals, the experimental data may be polluted by noise. In order to reduce the influence of noise, a digital low pass filter is designed with the cut-off frequencies being adjusted from 200 Hz to 1000 Hz , and the step responses are filtered.

3.2 Modeling method

The model parameters of the wrist force sensor are estimated by the least squares method [7]. As the oscillation attenuation of the sensor's dynamic response is slow, when the model response is compared with the actual response, it is we found out that the fitting precision is not high. At this time, the model parameters in the discrete domain are transformed into the continuous domain, and the natural frequency ω_n (or f_n) and damp ratio ξ are solved out. Then ξ is modified and transformed back to the discrete domain. The model response is obtained once again, and the modeling accuracy is improved.

3.3 Modeling results

The modeling results of six channels of a wrist force sensor (No. 1) are shown in Fig. 3-1 (a)～(f). In the figures, curve 1 expresses the actual response, and curve 2 expresses the model output. The performance indexes in the frequency domain of one sensor are shown in Table 3-1. In the dynamic experiments, we hung the weight with different kinds of strings, such as nylon string, badminton racket string and tennis racket string, and the strings were cut off at different positions, such as the center of above or under calibration test bench.

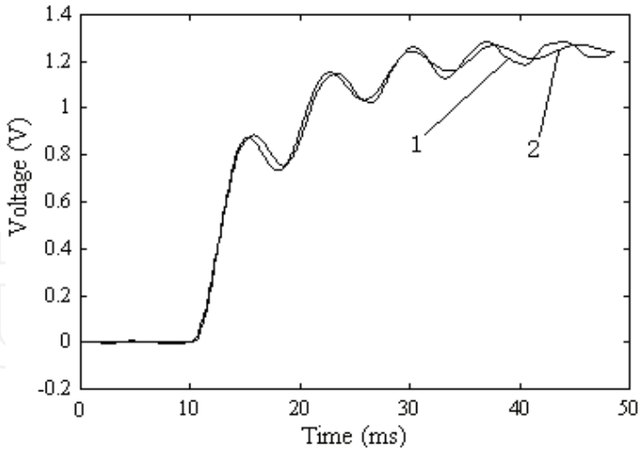

(a) Channel F_x

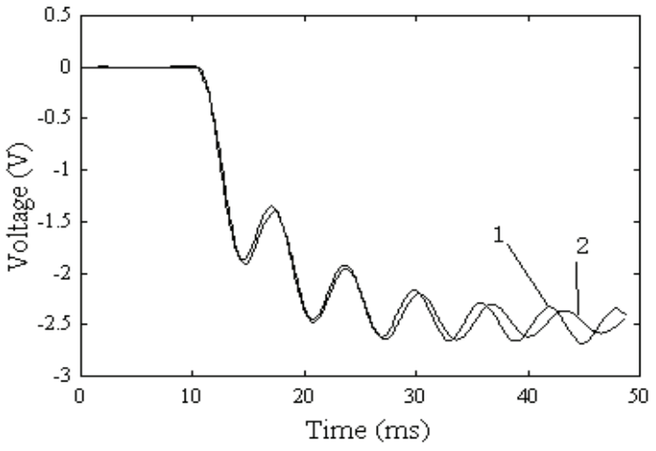

(b) Channel F_y

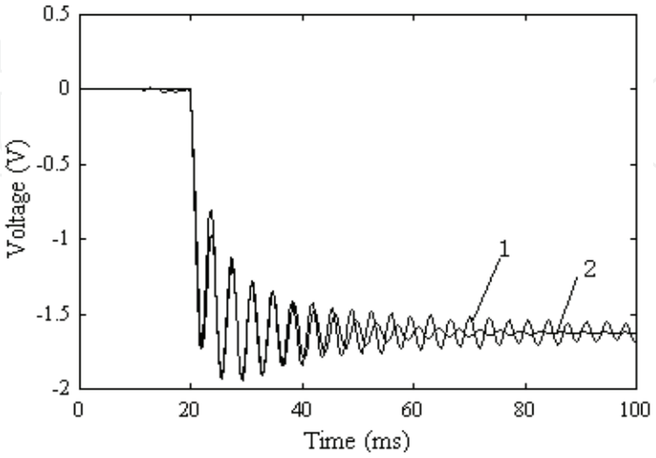

(c) Channel F_z

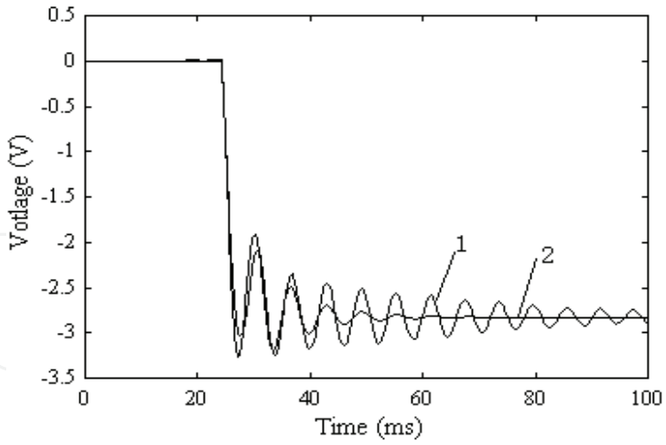

(d) Channel M_x

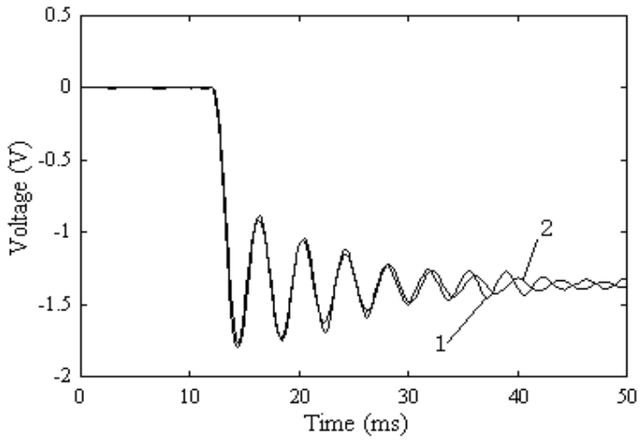

(e) Channel M_y

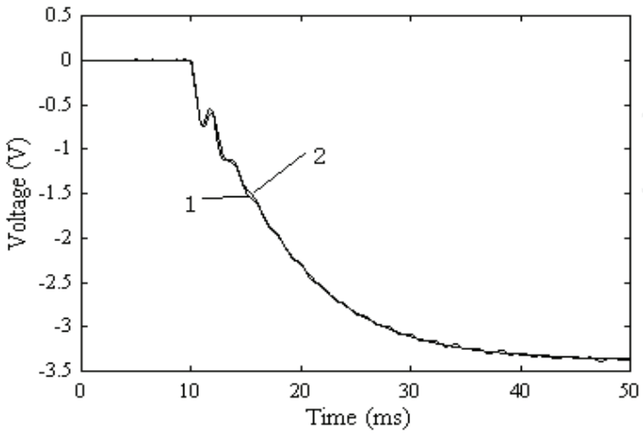

(f) Channel M_z

Fig. 3-1 Modeling results (1) Actual response, (2) model response.

	ξ	f_n	Remarks
F_x	0.105127	130.095841	Cutting on side
F_y	0.059806	150.582778	Cutting on side
F_z	0.0251005	274.554810	Cutting in middle
	0.0392930	266.282844	Cutting on side
M_x	0.162782	148.175903	Cutting on side
M_y	0.066125	127.218132	Cutting on side
M_z	0.267158	524.732768	Cutting in middle
	0.107061	483.605486	Cutting on side

Table 3-1 Performance indexes of sensor in frequency domain

4. Dynamic compensation

The experimental results showed that the step response time of the wrist force sensor varied from 20 ms to 100 ms (error being within ± 10 %), which was not satisfying with some applications, so the dynamic compensation methods and system should be studied and developed to speed the sensor dynamic responses. Firstly, the dynamic compensation system should be designed using the system identification method, pole-zero configuration or artificial neural network. Secondly, the dynamic compensation system should be implemented with DSP chip, which includes six compensating devices.

4.1 Design principle of dynamic compensation device

A designing method of the dynamic compensation device was proposed based on FLANN (Function link artificial neural network) by us. FLANN has the excellent ability to approximate many functions [8]. Patra et al. utilized FLANN to estimate and correct the static nonlinearly of pressure sensor, but FLANN has not been used for studying the dynamic characteristics of sensors at that time [9,10]. We constructed the structure of the neural network, made it be of time delay and present the dynamic characteristic. It is supposed that $u(k)$ is the input signal of sensor, i.e. the measured signal, that $y(k)$ is the output signal, and that $u'(k)$ is the output signal of the dynamic compensating device attached to the sensor. In order to shorten the time of dynamic response and make the measured signal reappear accurately, $u'(k)$should be approximate to $u(k)$ as closely as possible. The dynamic inverse model of the sensor is established using the method of FLANN off-line, and the inverse model is used as the model of the dynamic compensation device. In designing, both $u(k)$ and $y(k)$ are used as the input of the network, and $u(k)$ is regarded as the reference output signal of the compensation device. A schematic diagram of training is shown in Fig. 4-1. Assuming m=2 and n=3, where m refers to the delay step number of $u(k)$ and n refers to the delay step number of $y(k)$, so as to perform real time processing and make the realization be easy, the training equation of the network are written as

$$u^{'}(k) = \begin{matrix} W_0(k)y(k) + W_1(k)y(k-1) + W_2(k)y(k-2) + W_3(k)u(k-1) \\ +W_4(k)u(k-2) \end{matrix} \tag{4.1}$$

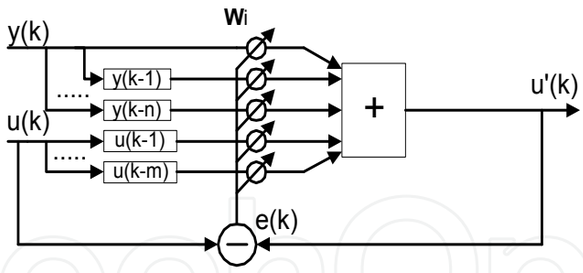

Fig. 4-1 Design schematic of dynamic compensating device by FLANN

Where W_i are the weights of the network, i.e. the model coefficients of the dynamic compensation device, k is the point number of data.
The error is

$$e(k) = u(k) - u^{'}(k) \tag{4.2}$$

The weight updating equations are given by

$$W_n(k+1) = W_n(k) + \alpha e(k) y(k-n) \quad (n = 0,1,2) \tag{4.3}$$

$$W_{m+2}(k+1) = W_{m+2}(k) + \alpha e(k) u(k-m-2) \quad (m = 1,2) \tag{4.4}$$

where the learning constant α governs the stability and the rate of convergence. If the value of α is too small, the speed of convergence is slow. If the value of α is too large, the result may diverge. Generally speaking, the value of α varies from 0 to 1. The simulation results show that it is suitable to set α about 0.1 for our case. After training of many times, when the average mean square error attains a minimum value, the obtained weights are the coefficients of the compensation device.
At the beginning of the on-line compensation, we suppose $u^{'}(k) = y(k)$, where k =0,1,2, and $u(k)$ is replaced by the output feedback $u^{'}(k)$. The equation of dynamic compensating is

$$u^{'}(k) = W_0 y(k) + W_1 y(k-1) + W_2 y(k-2) + W_3 u^{'}(k-1) + W_4 u^{'}(k-2) \ (k \geq 3) \tag{4.5}$$

It should be noted that the designing equations mentioned above are used for one channel of the wrist force sensor, and the equations for other channels are on the analogy of the above equations.

4.2 Design procedure of dynamic compensation device

1. An ideal equivalent measurement system including the sensor and the dynamic compensation device is constructed by adjustment the damp ratio and natural frequency.
2. The exciting signal (constructed or practical) is inputted, and the dynamic response of the equivalent measurement system is obtained.
3. Based on the dynamic responses of both the wrist force sensor and the equivalent measurement system, a dynamic compensation device is designed.

4. The dynamic response of the wrist force sensor is corrected.
5. In the light of the effects of compensation, the dynamic compensation devices are improved until the requirement is satisfied.

4.3 Dynamic compensation system

1. Realization of the dynamic compensation system

This dynamic compensation system consists of six dynamic compensating devices for six directions of the wrist force sensor, and the data acquisition, decoupling, dynamic compensating and output can be performed with the system.

Fig. 4-2 shows the hardware block of the dynamic compensation system. This system mainly includes an ADSP-2181 EZ-KIT Lite, an analog input part, an output part and the logic control circuit. The analog input part consists of eight sampling and holding circuits (S/H), a multiplexer (MUX), an amplifier (AMP) and an analog-to-digital converter (A/D). The output part contains six digital to analog converters (D/A) and six RC filters. The logic control circuit mainly consists of a decoder. The ADSP-2181 EZ-KIT Lite board is a minimal implementation system of an ADSP-2181 processor designed by ADI Corporation, and mainly includes an ADSP-2181, an EPROM and a serial communication port. The outputs of eight channels of the wrist force sensor are connected to the inputs of eight S/Hs. Whether the sampling mode is switched to the holding mode is controlled by ADSP-2181 based on the sampling frequency. Eight channel signals are switched and connected sequentially by the MUX, amplified by the AMP, and sent to the A/D. A busy pin of the A/D is connected to a programmable input/output pin. The ADSP-2181 determines the reading time according to the status of the busy pin.

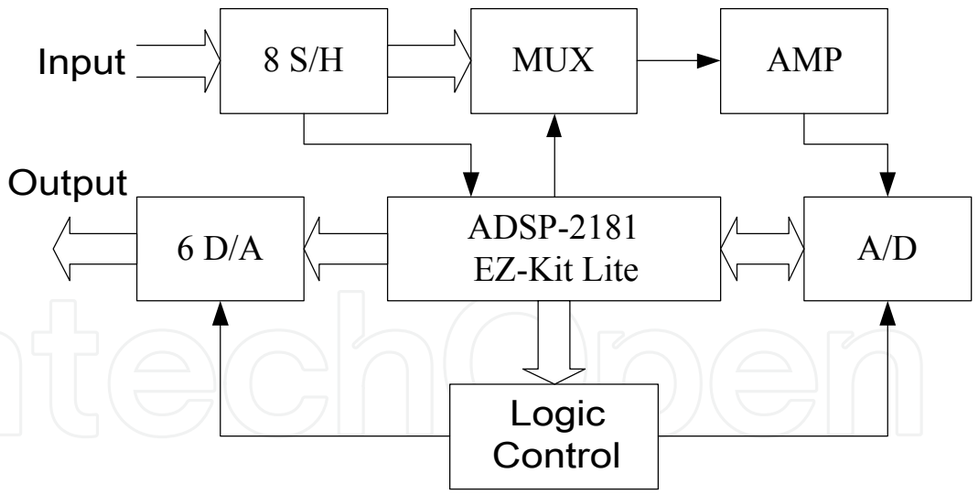

Fig. 4-2 Schematic block digram of dynamic compensating system

After eight channel signals are acquired by the ADSP-2181 at the same time, they are decoupled statically to be six channel signals, i.e. F_x, F_y, F_z, M_x, M_y and M_z. Then the six channel signals are compensated dynamically, and output by six D/As. Under the program control of the ADSP-2181, the logic control circuit determines the chip selection of A/D and D/A.

The software design of the system includes a data acquisition module, a data processing module and a result output module. The sampling interval of the system is determined by

the interrupt of the timer, and is 50 μs or 250 μs so as to sample enough data in the sensor's dynamic response process. When the power is applied to the system, it starts initialization, and then enters the state of waiting for interruption. When the timer generates an interruption, the system begins a circle of data acquisition, processing and output. In one sampling period, the eight channel signals of the same time are acquired, decoupled statically to become six channel signals, then compensated dynamically, and output. The system runs the program continuously in this way.

2. Experimental results of the dynamic compensation system

The dynamic compensation system was connected to the wrist force sensor, and the dynamic experiments of step response were conducted to verify the effectiveness of dynamic compensation. The dynamic compensation results of six channels of a wrist force sensor (No. 3) are shown in Fig. 4-3 (a)～(f). In figures, curve 1 was the dynamic response of the wrist force sensor, and curve 2 is the output of the dynamic compensation system. The compensation coefficients of six channels were shown in Table II. The experimental results indicate that the adjusting time (within $\pm$10 error of steady status) of dynamic response of the wrist force sensor is less than 5 ms, i. e. the adjusting time is reduced to less than 25%, and the dynamic performance indexes is greatly improved via dynamic compensation.

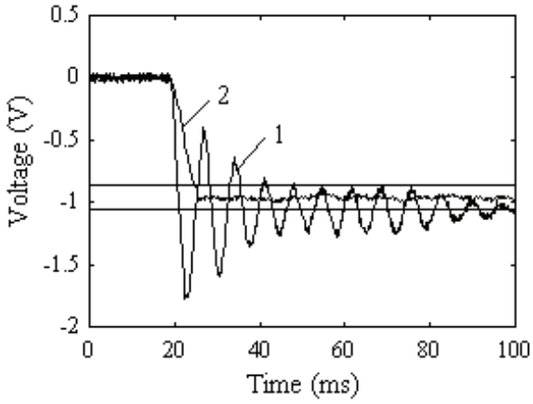

(a) Channel F_x

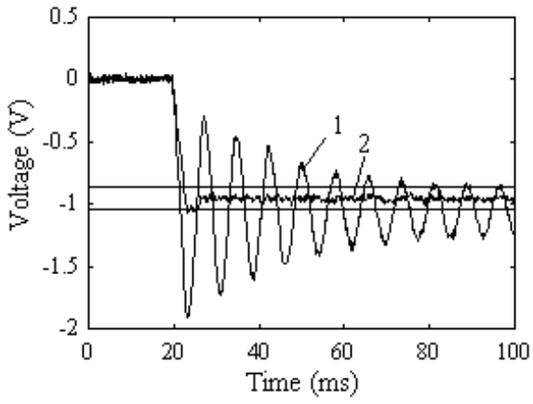

(b) Channel F_y

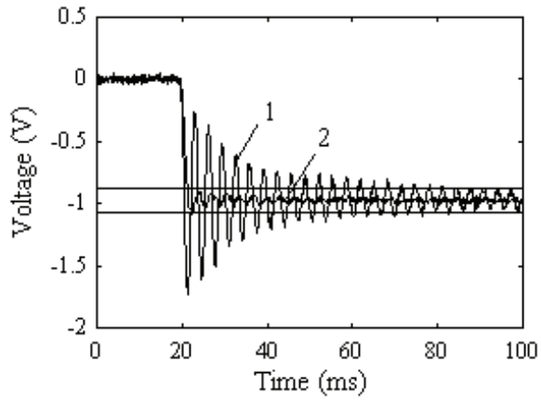

(c) Channel F_z

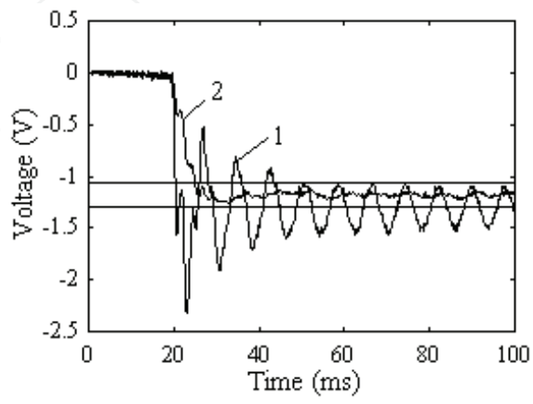

(d) Channel M_x

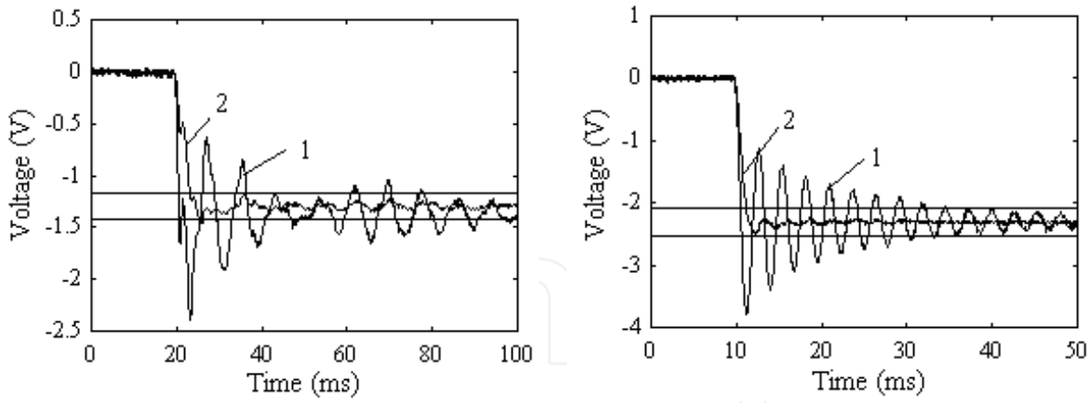

(e) Channel M_y (f) Channel M_z

Fig. 4-3 Experiment results (1) dynamic response of sensor, (2) output of dynamic compensating system.

	F_x	F_y	F_z	M_x	M_y	M_z
W_0	0.264231	0.959694	0.777428	0.251256	0.359567	0.920652
W_1	-0.525321	-1.915169	-1.541528	-0.4987790	-0.713234	-1.818204
W_2	0.261612	0.957071	0.772072	0.248014	0.354212	0.909576
W_3	1.966720	1.956619	1.871834	1.969605	1.970583	1.846556
W_4	-0.967239	-0.958209	-0.879801	-0.970085	-0.971131	-0.858568

Table 4-1 Coefficients of dynamic compensating system

5. Dynamic decoupling-compensation

There are dynamic couples among various channels of multi-axis force and torque sensors because the elastic body of the sensor is an integer structure and the interaction of various channels cannot be avoided completely. In addition, due to their small damped ratio and low natural frequency, the sensors dynamic response is slow, and the time to reach steady state is long. Both dynamic coupling and slow dynamic response are two main factors affecting the dynamic performances of sensors. We proposed the dynamic compensating and decoupling methods of multi-force sensors, constructed four types of dynamic decoupling and compensating networks, gave the design procedures and determines the order and parameters of the networks. The parameters of the networks are determined using the method based on FLANN. The dynamic decoupling and compensating results of a wrist force sensor have proved the methods to be correct and effective.

5.1 Structures of dynamic decoupling and compensating networks

The different places of compensating part result in different structure of dynamic decoupling and compensating network. In general, the compensating part is not put in front of decoupling part; otherwise it will make the design of decoupling part complex. The structure in which decoupling is done first and then compensation is carried out is called a serial decoupling and compensating network .The structure in which decoupling and

compensation are completed at the same time is called a parallel network. Taking two dimensional force sensor as an example, the structures of various networks are shown in Fig.5-1 (a)~ (b).

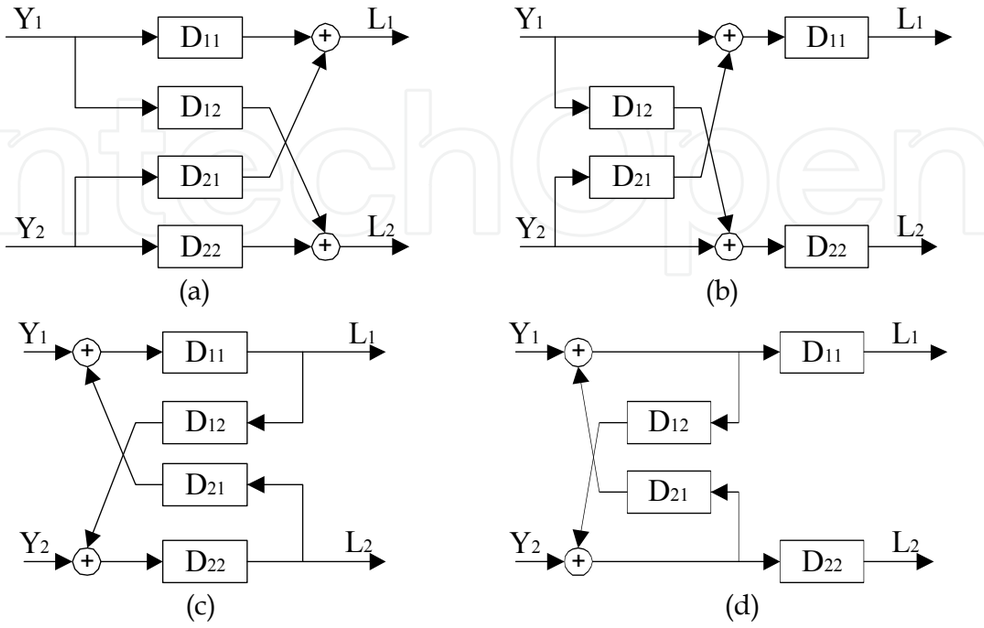

Fig. 5-1 Four kinds of network structures

In Fig. 5-1, (a) expresses the P parallel decoupling and compensating network (PPDCN), (b) is the P serial decoupling and compensating network (VPDCN), (c) describes the V Parallel Decoupling and Compensation Network (VPDCN),(d) is the V Serial Decoupling and Compensation Network (VSDCN). In figures, Y_i are the outputs of sensor, and L_i are the outputs of decoupling and compensating network.

5.2 Designs of dynamic decoupling and compensating networks

1. Design of PSDCN

The design procedure of PSDCN includes two steps. At first the decoupling part is designed, and then the compensating part is done. The design goal of decoupling part is to make the elements of non-main diagonal line in the matrix which is product of sensor transfer function matrix and decoupling matrix be zero. The design goal of compensating part is to make the compensating matrix equal to inverse of product matrix obtained by multiplying the sensor transfer function matrix and the decoupling matrix. For n-dimensional sensor, the decoupling matrix D_{psd} and compensating matrix D_{psc} in PSDCN respectively are given by equation (5.1).

$$D_{psd}=\begin{bmatrix} 1 & D_{12} & \dots & D_{1n} \\ D_{21} & 1 & \dots & D_{2n} \\ \dots\dots & & & \\ D_{n1} & D_{n2} & \dots & 1 \end{bmatrix} \quad D_{psc}=\begin{bmatrix} D_{11} & 1 & \dots & 1 \\ 1 & D_{22} & \dots & 1 \\ \dots\dots & & & \\ 1 & 1 & \dots & D_{nn} \end{bmatrix} \tag{5.1}$$

To decouple completely, we must have

$$G \cdot D_{psd} \cdot D_{psc} = I \tag{5.2}$$

$$\text{Therefore} \quad D_{psd} \cdot D_{psc} = \begin{bmatrix} D_{11} & D_{12}D_{22} & \dots & D_{1n}D_{nn} \\ D_{21}D_{11} & D_{22} & \dots & D_{2n}D_{nn} \\ \dots\dots & & & \\ D_{n1}D_{11} & D_{n2}D_{22} & \dots & D_{nn} \end{bmatrix} = \frac{1}{|G|} G^* \tag{5.3}$$

Where, $|G|$ is the determinant matrix of sensor transfer function G, and G^* is the companion matrix of G.

To make the corresponding elements in equation (5.3) equal, the elements of D_{psd} and D_{psc} are resolved as follows.

$$D_{ii} = \frac{G_{ii}^*}{|G|}, \quad D_{ij} = \frac{G_{ji}^*}{|G| \cdot D_{jj}} \qquad (i = 1,2,...,n; j = 1,2,...,n; i \neq j) \tag{5.4}$$

2. Design of PPDCN

Designing PPDCN is used by a direct method of solving inverse matrix. Supposing PPDCN to be the inverse matrix of sensor transfer function, the decoupling and compensating matrix D_{ppdc} is given by equation (5.5).

$$D_{ppdc} = \begin{bmatrix} D_{11} & D_{12} & \dots & D_{1n} \\ D_{21} & D_{22} & \dots & D_{2n} \\ \dots\dots & & & \\ D_{n1} & D_{n2} & \dots & D_{nn} \end{bmatrix} \tag{5.5}$$

If D_{ppdc} is equal to the inverse matrix of sensor transfer function, the elements of D_{ppdc} can be solved.

$$D_{ij} = \frac{G_{ji}^*}{|G|}, (i = 1,2,...,n; j = 1,2,...n;) \tag{5.6}$$

3. Design of VSDCN

The mathematical equations of VSDCN are given as follows.

$$L_i = Y_i + \sum_{\substack{j=1 \\ j \neq i}}^{n} D_{ij} L_j \ , (i = 1,2,...,n) \tag{5.7}$$

We can obtain

$$Y_i = L_i - \sum_{\substack{j=1 \\ j \neq i}}^{n} D_{ij} L_j , (i = 1,2,...,n) \tag{5.8}$$

Equation (5.7) can be written into a matrix form.

$$Y = LT \tag{5.9}$$

Here, Y and L are line vectors; T is a matrix described in equation (5.10).

$$T = \begin{bmatrix} 1 & -D_{12} & \dots & -D_{1n} \\ -D_{21} & 1 & \dots & -D_{2n} \\ \dots & & & \dots \\ -D_{n1} & -D_{n2} & \dots & 1 \end{bmatrix} \tag{5.10}$$

If T is the regular matrix, the decoupling matrix D_{vsd} of VSDCN is given by

$$D_{vsd} = T^{-1} \tag{5.11}$$

To reach decoupling and compensation completely, the following equation must be satisfied.

$$G \cdot D_{vsd} \cdot D_{vsc} = I \tag{5.12}$$

Where D_{vsc} is a compensating matrix.
Equation (5.12) yields

$$D_{vsd} \cdot D_{vsc} = G^{-1} \tag{5.13}$$

Therefore

$$G = D_{vsc}^{-1} \cdot T = \begin{bmatrix} \frac{1}{D_{11}} & -\frac{D_{12}}{D_{11}} & \dots & -\frac{D_{1n}}{D_{11}} \\ -\frac{D_{21}}{D_{22}} & \frac{1}{D_{22}} & \dots & -\frac{D_{2n}}{D_{22}} \\ \dots\dots & & & \\ -\frac{D_{n1}}{D_{nn}} & -\frac{D_{n2}}{D_{nn}} & \dots & \frac{1}{D_{nn}} \end{bmatrix} \tag{5.14}$$

The model of VSDCN can be obtained from solving equation (5.14).

$$D_{ii} = \frac{1}{G_{ii}}, D_{ij} = -\frac{G_{ij}}{G_{ii}}, (i = 1,2,...,n; j = 1,2,...,n; i \neq j) \tag{5.15}$$

4. Design of VPDCN

The mathematical equations of VPDCN are described by

$$L_i = D_{ii}(Y_i + \sum_{\substack{j=1 \\ j \neq i}}^{n} D_{ij} L_j), (i = 1,2,...,n) \tag{5.16}$$

From equation (5.16), we obtain

$$Y_i = \frac{L_i}{D_{ii}} - \sum_{\substack{j=1 \\ j \neq i}}^{n} D_{ij} L_j \ , (i = 1, 2, ..., n) \tag{5.17}$$

Equation (5.17) can be written in a matrix form

$$Y = LT \tag{5.18}$$

Where, Y and L are line vectors, and T is a $n \times n$ matrix.

$$T = \begin{bmatrix} \frac{1}{D_{11}} & -D_{12} & ... & -D_{1n} \\ -D_{21} & \frac{1}{D_{22}} & ... & -D_{2n} \\ ..... & & & \\ -D_{n1} & -D_{n2} & ... & \frac{1}{D_{nn}} \end{bmatrix} \tag{5.19}$$

If T is the regular matrix, the D_{vpdc} of VPDCN is

$$D_{vpdc} = T^{-1} \tag{5.20}$$

In order to achieve decoupling and compensation, we have

$$G \cdot D_{vpdc} = I \tag{5.21}$$

Therefore

$$G = D_{vpdc}{}^{-1} = (T^{-1})^{-1} = T \tag{5.22}$$

The model of VPDCN can be solved from equation (5.22).

$$D_{ii} = \frac{1}{G_{ii}}, D_{ij} = -G_{ij} \qquad (i = 1, 2, ..., n; j = 1, 2, ..., n; i \neq j) \tag{5.23}$$

5. Designs of decoupling and compensating networks for non-minimum phase system

If the wrist force sensor is a non-minimum phase system, the above-mentioned method which designs the dynamic decoupling and compensating networks will result in the result to be unsteady. Therefore, before the dynamic decoupling and compensating networks are designed, the dynamic compensating digital filters are designed for non-coupled paths. The design of dynamic compensating digital filter can adopt the pole-zero configuration method or system identification method [11, 12]. The result F of dynamic compensation for non-coupled paths is

$$F = \begin{bmatrix} f_{11} g_{11} & 0 & ... & 0 \\ 0 & f_{22} g_{22} & ... & 0 \\ ..... & & & \\ 0 & 0 & ... & f_{nn} g_{nn} \end{bmatrix} \tag{5.24}$$

Where, g_{ii} (i=1,2,…,n) is the transfer function for the ith path of sensor, f_{ii} (i=1,2,⋯,n) is the transfer function of dynamic compensating digital filter for the ith path of sensor.
In the design process of four kinds of dynamic decoupling and compensating networks, supposed the product of sensor transfer function and the matrix of decoupling and compensation to be equal to F, the corresponding decoupling and compensating network are obtained. The deducing procedure is similar with the previous section. The models of dynamic decoupling and compensating networks are as follows.
(1) PSDCN

$$D_{ii} = \frac{f_{ii} \cdot G_{ii}^{*} G_{ii}}{|G|}, \quad D_{ij} = \frac{G_{ji}^{*}}{|G| \cdot D_{jj}} \quad (i = 1,2,...,n; j = 1,2,...n; i \neq j) \tag{5.25}$$

(2) PPDCN

$$D_{ii} = \frac{f_{ii} \cdot G_{ii}^{*} G_{ii}}{|G|}, D_{ij} = \frac{G_{ji}^{*} f_{ii} G_{ii}}{|G|} \quad i = 1,2,...,n; j = 1,2,...n; i \neq j \tag{5.26}$$

(3) VSDCN

$$D_{ii} = f_{ii}, D_{ij} = -\frac{G_{ij}}{G_{ii}}, (i = 1,2,...,n; j = 1,2,...,n; i \neq j) \tag{5.27}$$

(4) VPDCN

$$D_{ii} = f_{ii}, D_{ij} = -\frac{G_{ij}}{f_{ii} G_{ii}}, (i = 1,2,...,n; j = 1,2,...,n; i \neq j) \tag{5.28}$$

5.3 Determination of orders and parameters

A FLANN-based method is used to determine the orders and parameters of the dynamic decoupling and compensating network. The system identification method can also been used to do this work, but it sometimes makes the model orders too high or decoupling and compensating results divergent because of modeling error. The FLANN method overcomes these shortcomings.
The designs of decoupling parts in PSDCN, VSDCN and VPDCN have nothing to do with the mix output signal of sensor, which includes non-coupled and coupled output signals. Therefore using input and output signals of sensor under no coupled condition at first sets up the models of decoupling parts. In design process of compensating part, the decoupling model is used for decoupling coupled signal, and then the compensating parts are designed in according with decoupled signal. Thus it can bring decoupling error in the design of compensating parts, and correct decoupling error in the design of compensating parts.
Designing PSDCN and VSDCN can adopt the system identification method or the FLANN method. Designing VPDCN only utilizes the FLANN method because it is a parallel structure with internal feedback, and modeling error may result in divergent. Designing PPDCN is complex, the models of compensating parts for non-coupled paths are set up at first by using the input and output signals of sensor under no coupled condition. The models of decoupling parts are trained by adjusting the difference between the

compensating result of mix output signal and input signal. Thus we can bring the compensating error in the design of decoupling part, and the compensating error is corrected in the decoupling part.

Suppose the input signals of sensor are $X_i(k)$; the output signals are $Y_i(k)$. The $X_i(k-1),...,\ X_i(k-r), Y_i(k-1),...,Y_i(k-s)$ are obtained by the functional expansion technique, which are used as the inputs of FLANN. The k expresses number of data, $k=1,...,N$. The inputs are weighted and summed, and the output $L_i(k)$ are yielded. The difference between $L_i(k)$ and $X_i(k)$ is regarded as error $e_i(k)$ to adjust the weights $W_i(k)$ of FLANN. A schematic diagram of FLANN for determining parameters is shown in Fig.5-2. An equation describing the neural algorithm can be written as

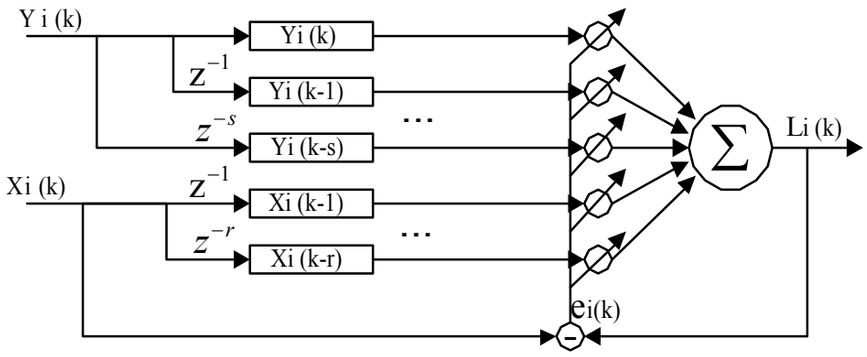

Fig. 5-2 Schematic of modeling by FLANN

$$L_i(k)=\sum_{p=1}^{r} w(j)X_i(k-p)+\sum_{q=1}^{s} w(q+r+1)Y_i(k-q) \tag{5.29}$$

The error is

$$e_i(k)=X_i(k)-L_i(k) \tag{5.30}$$

The weight update equations are given by

$$w_i(p)=w_i(p)+\alpha\cdot e_i(k)X_i(k-p)$$

$$w_i(q+r+1)=w_i(q+r+1)+\alpha\cdot e_i(k)Y_i(k-q) \tag{5.31}$$

Where $L_i(k), Y_i(k), e_i(k), W_i(k)$ stand for the desired output of the ith path, estimating output, error and the pth or the qth linking weight in the kth step of the FLANN. The α denotes the learning constant which connects with the stability and the rate of convergence, usually is selected about 0.1. In training process, initial values of weights are chosen about 0.1. After training for many times, when the average mean square error achieved a minimum value, the weights of FLANN are the parameters of dynamic decoupling and compensating network.

5.4 Dynamic decoupling and compensating results

1. Evaluating indexes

To evaluate the decoupling and compensating results, the indexes are adopted as the follows.

(1) The variance is

$$\sigma = \sqrt{\frac{(L_i - X_i)^2}{N-1}} \tag{5.32}$$

where X_i are the input signals of sensor, L_i are corresponding decoupling and compensating output signals, and N is total number of data.

(2) The relative error is

$$e_r = \frac{(L_i - X_i)_{\max}}{|X_i|_{\max}} \times 100\% \tag{5.33}$$

2. Results of simulation

In order to examine the decoupling and compensating methods, we carry out the simulation. The results of simulation indicate that the VSDCN and VPDCN can achieve the good effectiveness, but the results of PSDCN and PPDCN have error because these methods use the low order model to substitute for the high order model.

3. Dynamic decoupling and compensating result of wrist force sensor

We decouple and compensate the dynamic output signals of wrist force sensor. The sensor is a six-axis device, i.e. n=6, the decoupling parts of PSDCN and PPDCN are very complex with high order. For examples, on the assumption that the model order of element in transfer function matrix is 3, the order of decoupling and compensating model in PPDCN will high to 33, so it will result in the bad convergence and a big error because of simplification. In generally, PSDCN and PPDCN can only be used for the dimensional number less than 3.

When the dimensional number larger than 3, VSDCN and VPDCN can only be used. The models of these networks do not vary with the number of variables, so do not have the problem of over-high order. For the wrist force sensor, we prefer VSDCN and VPDCN. In brief, we only introduce the result of VSDCN. The decoupling and compensating results between direction Z and direction X is shown in Fig.5-3 (a) and (b). The decoupling and compensating results between direction Z and direction Y is shown in Fig.5-4 (a) and (b). In the figures the orders of both decoupling and compensating models are 3, curve 1 expresses the input signal of sensor, curve 2 expresses the decoupled and compensated result.

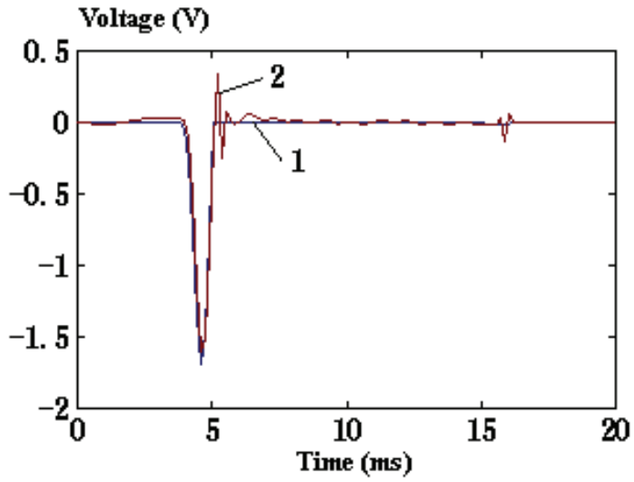

Fig. 5-3 (a) Decoupling and compensating result of direction Z

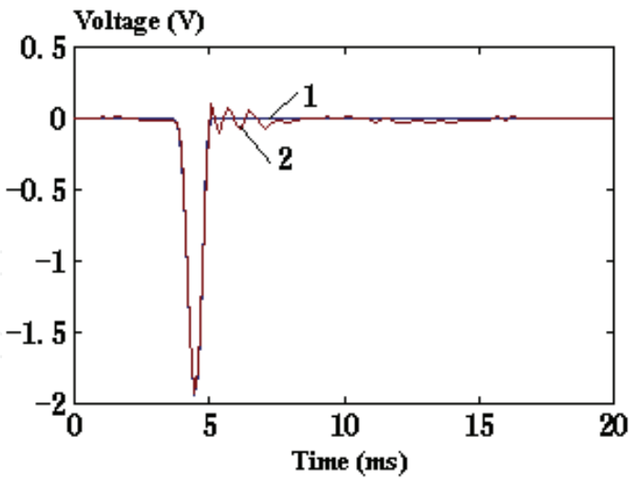

Fig. 5-3 (b) Decoupling and compensating result of direction X

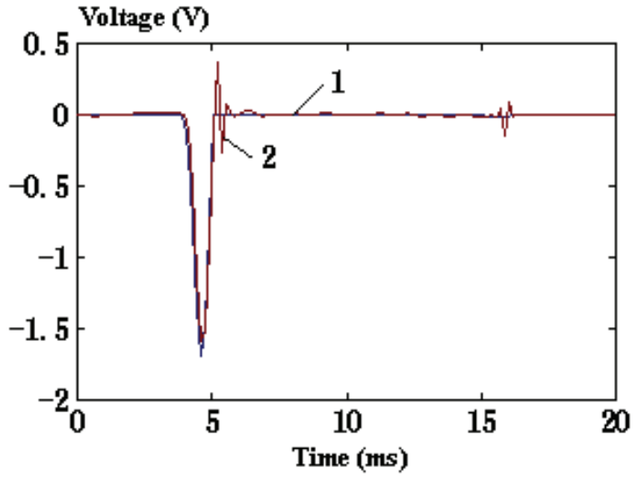

Fig. 5-4 (a) Decoupling and compensating result of direction Z

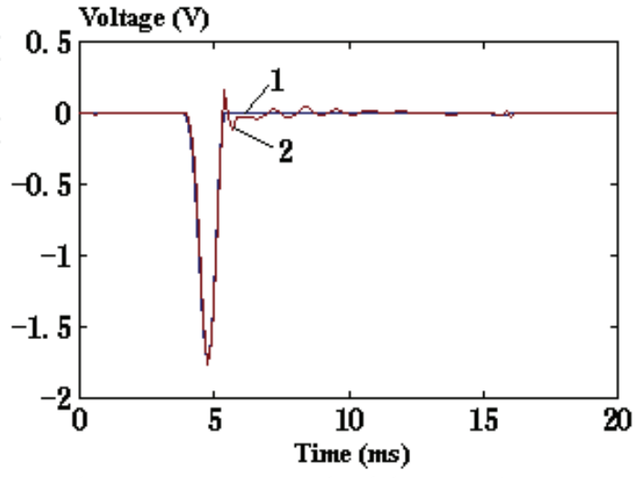

Fig. 5-4 (b) Decoupling and compensating result of direction Y

Comparisons of the decoupling and compensating errors between direction Z and direction X is seen in Table 5-1. Comparisons of the decoupling and compensating errors between direction Z and direction Y are seen in Table 5-2. Analyzing Table 1 and Table 2, the results of PSDCN are the worst and the results of VSDCN are the best.

Error indexes	PSDCN	PPDCN	VSDCN	VPDCN
σ in direction Z	0.0880	0.0567	0.0543	0.0668
e_r in direction Z	18.50%	19.35%	15.70%	14.25%
σ in direction X	0.0717	0.0276	0.0270	0.0538
e_r in direction X	19.71%	5.62%	5.53%	10.54%

Table 5-1 Comparisons of the decoupling and compensating errors between direction Z and direction X

Error indexes	PSDCN	PPDCN	VSDCN	VPDCN
σ in direction Z	0.0731	0.0585	0.0586	0.0946
e_r in direction Z	18.91%	20.59%	21.60%	25.10%
σ in direction Y	0.0960	0.0449	0.0301	0.0479
e_r in direction Y	23.70%	13.37%	9.23%	13.10%

Table 5-2 Comparisons of the decoupling and compensating errors between direction Z and direction Y

4. Conclusions

Four kinds of decoupling and compensating networks are presented in this section. Analyzing from principle, compared with PSDCN and PPDCN, VSDCN and VPDCN are more concise, they have definite physical meaning and can achieve full decoupling and compensation. Judging from the construction, parallel networks are better than serial networks because the decoupling and compensation are combined into one unit.

The decoupling and compensating error are caused mainly by the following reasons. (a) There are modeling errors in four kinds of networks. (b) The simplification of molder result in the errors in PSDCN and PPDCN.

The decoupling and compensating methods can also be applied to other multi-axis force sensors.

6. Nonlinear dynamic characteristics

There is the non-linearity in the dynamic characteristics of sensors under some conditions. In order to describe accurately the dynamic behavior of sensors some researchers studied the nonlinear dynamic characteristics of sensors. Waldemar Minkina presented nonlinear models that adequately describe the dynamic state of temperature sensor within the temperature increase range [13,14]. Ping Wang et al. discussed the analysis of nonlinear dynamic state of accelerometer transducers and its applications in the dynamic modeling [15]. S. Beling et al. approximated the dynamic behavior of nonlinear gas sensors using the feed-forward neural networks [16]. Haixia Zhang et al. studied the transient process of the sensor probe, and developed a nonlinear model based on equivalent electrical circuit techniques [17]. Ke-Jun Xu et al. studied the nonlinear dynamic characteristics of the wrist

force sensor in the time and frequency domains [18,19]. These researches described the nonlinear dynamic models of sensors only using one block. On the basis of these models the nonlinear dynamic responses of sensors are compensated to improve the dynamic performances of sensors. Antonio Pardo et al. built a nonlinear inverse dynamic system to solve the non-linearity of gas sensing system [20]. Ke-Jun Xu et al. designed a dynamic compensating system for the wrist force sensor using FLANN [21]. The nonlinear dynamic compensations achieve good results under some certain conditions. Since the nonlinear dynamic system is not satisfied with the homogeneity and superposition, the dynamic compensations based on the above-mentioned nonlinear dynamic models are effective for the certain response of sensors, but are not suitable for different form and different amplitude responses of sensors.

6.1 Hammerstein model based modeling

Previous researchers present the nonlinear dynamic models of sensors only using a block, which make it difficulty to compensate the nonlinear dynamic responses of sensors. The models of sensors with the nonlinear dynamic characteristic may be divided into two blocks, that is, a nonlinear static part and a linear dynamic one. The linear dynamic part is first compensated and then the nonlinear static part is corrected. Thus the problems of previous nonlinear dynamic compensations of sensors are solved. In this section a Hammerstein model is adopted to describe the nonlinear dynamic models of sensors, and a one-stage identification algorithm is proposed to simplify the calculation. On this basis a two-step compensation method is present for the nonlinear dynamic responses of sensors.

1. Deduction of one-stage identification algorithm

The Hammerstein model is composed of a nonlinear static block $N(\cdot)$ followed by a linear dynamic one $h(t)$, which is shown in Fig. 6-1 [22,23]. The $u(t)$ and $y(t)$ are the input and output of the Hammerstein model respectively, $\xi(t)$ is white noise, and $x(t)$ stands for the output of nonlinear static block.

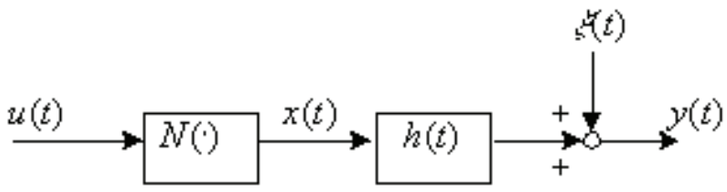

Fig. 6-1 Hammerstein model

Assuming the nonlinear static block can be approximated by a polynomial, and can be written as

$$N(\cdot) = \sum_{j=1}^{J} c_j u^j(t) \tag{6.1}$$

And

$$x(t) = N\left[u(t)\right] \tag{6.2}$$

The difference equation of the Hammerstein model is

$$A(q^{-1})y(k) = B(q^{-1})N\left[u(k)\right] + \xi(k) \tag{6.3}$$

Where

$$A(q^{-1}) = 1 + a_1 q^{-1} + \cdots + a_n q^{-n} \tag{6.4}$$

$$B(q^{-1}) = b_0 + b_1 q^{-1} + \cdots + b_m q^{-m} \tag{6.5}$$

$$N\left[u(k)\right] = \sum_{j=1}^{l} c_j u^j(k) \tag{6.6}$$

The transfer function of the linear dynamic block can be given as

$$H(z^{-1}) = \frac{b_0 + b_1 z^{-1} + \cdots + b_m z^{-m}}{1 + a_1 z^{-1} + \cdots + a_n z^{-n}}. \tag{6.7}$$

Considering Equations (6.3), (6.4), (6.5) and (6.6), we can obtain

$$y(k) = -\sum_{p=1}^{n} a_p y(k-p) + \sum_{j=1}^{l}\sum_{v=0}^{m} b_v c_j u^j(k-v) + \xi(k) \tag{6.8}$$

Assuming

$$w_{vj} = b_v c_j \qquad v = 0,1,\cdots m,\ j = 1,\cdots l\ . \tag{6.9}$$

Then Equation (6.8) becomes

$$y(k) = -\sum_{p=1}^{n} a_p y(k-p) + \sum_{j=1}^{l}\sum_{v=0}^{m} w_{vj} u^j(k-v) + \xi(k) \tag{6.10}$$

Equation (6.10) can also be expressed as

$$y(k) = \Phi^{\mathrm{T}}(k)\theta(k) + \xi(k) \tag{6.11}$$

Where

$$\theta(k) = [a_1, \cdots, a_n, w_{01}, \cdots, w_{m1}, \cdots, w_{0l}, \cdots, w_{ml}]^{\mathrm{T}}$$

$$\Phi(k) = [-y(k-1), \cdots, -y(k-n), \cdots, u(k), \cdots, u(k-m), \cdots, u^l(k), \cdots, u^l(k-m)]^{\mathrm{T}}$$

Equation (6.11) is a parameter model describing the relation between the input and output. The parameters of the model are obtained using the least square method (LSM) or the FLANN [24].

Assuming that the gain of steady state of the linear dynamic unit is 1, that is

$$H(\infty) = \frac{b_0 + \cdots + b_m}{1 + a_1 + \cdots + a_n} = 1 \tag{6.12}$$

Thus the gain of steady state of the nonlinear dynamic system stems from the nonlinear static block.

When $\forall j = 1, 2, \cdots, l$, we can obtain the following equation from Equation (6.9).

$$\sum_{v=0}^{m} w_{vj} = (b_0 + \cdots + b_m)c_j \quad v = 0, 1, \cdots m, j = 1, \cdots l \ . \tag{6.13}$$

Then

$$c_j = \frac{\sum_{v=0}^{m} w_{vj}}{b_0 + \cdots + b_m} = \frac{\sum_{v=0}^{m} w_{vj}}{1 + a_1 + \cdots + a_n} \tag{6.14}$$

Thus the coefficients of the nonlinear static block $c_1, \cdots, c_l$ are solved from $a_1, \cdots, a_n, w_{01}, \cdots, w_{ml}$ obtained by identification. On this basis we can yield

$$b_v = \frac{w_{vj}}{c_j} \quad v = 0, 1, \cdots m, j = 1, \cdots l \ . \tag{6.15}$$

Now the coefficients of the linear dynamic unit are also obtained. Due to the inevitable iterative error of the LSM or the FLANN, b_v $(v = 0, 1, \cdots m)$ obtained from Equation (6.15) may not satisfy Equation (6.12). However, the dynamic characteristics of a linear system, such as what can be expressed as Equation (6.7), mainly depend on its poles instead of zeros. While b_v $(v = 0, 1, \cdots m)$ is the zero, and has little effect on the dynamic characteristics of a system. Therefore Equation (6.7) can also be expressed as

$$H(z^{-1}) = \frac{A}{1 + a_1 z^{-1} + \cdots + a_2 z^{-n}} \tag{6.16}$$

Where

$$A = 1 + \sum_{i=1}^{n} a_i \tag{6.17}$$

This viewpoint may be proved as the following. Assuming $a_1 = -1.95974$, $a_2 = 0.98681$, $b_0 = 0.00677$, $b_1 = 0.01353, b_2 = 0.00677$, and $m = n = 2$, the step responses of the system are obtained from Equations (6.7) and (6.16) respectively, and are shown in Fig. 6-2. Two response curves are identical. Even if we have not solved the parameters b_v $(v = 0, 1, \cdots m)$, the dynamic characteristics of the sensor can also be obtained. Therefore, using one-stage identification method, we can obtain the coefficients of both the nonlinear static block and the linear dynamic unit according to the inputs and outputs of the nonlinear dynamic system.

2. Simulations of modeling

In order to examine the one-stage identification algorithm, the simulations are carried out. The step signal and impulse signal are chosen as input signals of modeling because they are usually applied to the experimental calibrations of sensors. Since a second-degree polynomial is commonly used in describing the nonlinear static characteristics of sensors in practice engineering, and a second-order linear dynamic unit is often admitted, we make our simulations based on the second-degree nonlinear static model and the second-order linear dynamic model. So let $m = n = 2$ in Equations (6-4) and (6-5), and $l = 2$ in Equation

(6-6), then a_1 , a_2 , b_0 , b_1 , c_1 and c_2 are parameters that will be estimated. We should first obtain a_1 , a_2 , $w_{01},\cdots,w_{22}$ through Equation (6-11).

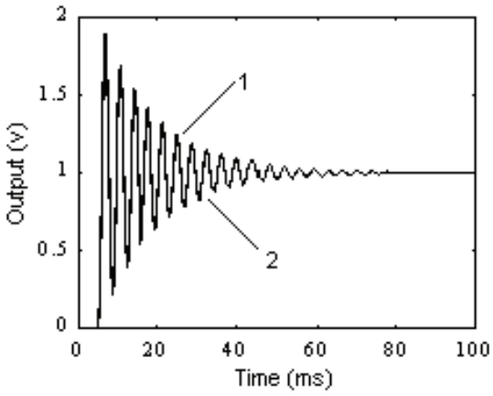

Fig. 6-2 Comparison of two response curves: (1) step response of Equ.(6-7), and (2) step response of Equ.(6-16).

Suppose a nonlinear static subsystem is

$$x(k) = u(k) + 0.5u^2(k) \tag{6.18}$$

A linear dynamic unit is given by

$$y(k) = 1.95974y(k-1) - 0.98681y(k-2)$$

$$+0.00667x(k) + 0.01353x(k-1) + 0.00667x(k-2) \tag{6.19}$$

A step input signal and a nonlinear dynamic response of the system are shown in Fig. 6-3. According to the inputs and outputs of the system, $a_1, a_2, w_{01},\cdots,w_{22}$, parameters in equation (6.11), are obtained using the LSM. Afterwards b_0, b_1, b_2, c_1, c_2 can be easily obtained through Equations (6.14) and (6.15). Thus a nonlinear dynamic model is set up using the one-stage identification algorithm. The response of this model is compared with that of the supposed system which is shown in Fig. 6-4. The supposed and identified parameters are listed in Table 6-1.

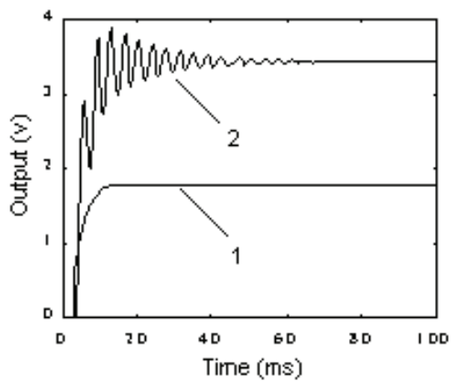

Fig. 6-3 Step input and supposed nonlinear dynamic response: (1) step input, and (2) nonlinear dynamic response .

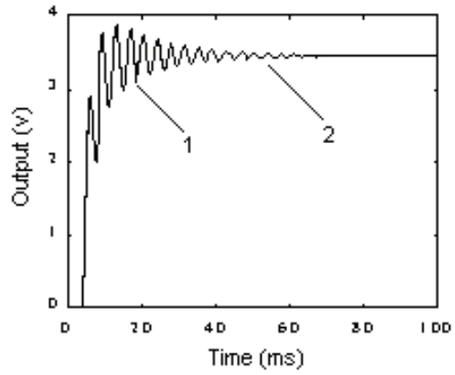

Fig. 6-4 Comparison of identification result and supposed response: (1) supposed response, and (2) identification result.

Parameter	a_1	a_2	b_0	b_1	b_2	c_1	c_2
Supposed	-1.95974	0.98681	0.00677	0.01353	0.00677	1.00	0.50
Identified	-1.95971	0.98679	0.00437	0.01323	0.00948	0.99663	0.50188

Table 6-1 Comparison between supposed and identified parameters

The simulation results of the impulse signal are shown in Fig. 6-5 and Fig. 6-6. The supposed and identified parameters are listed in Table 6-2.

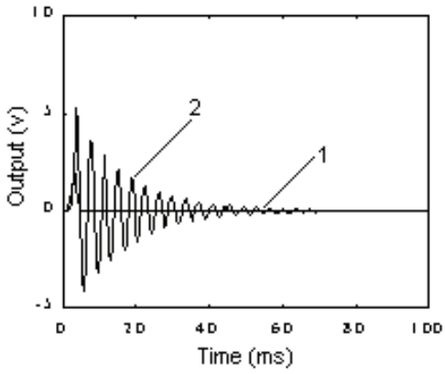

Fig. 6-5 Impulse input and nonlinear dynamic response: (1) impulse input, and (2) nonlinear dynamic response.

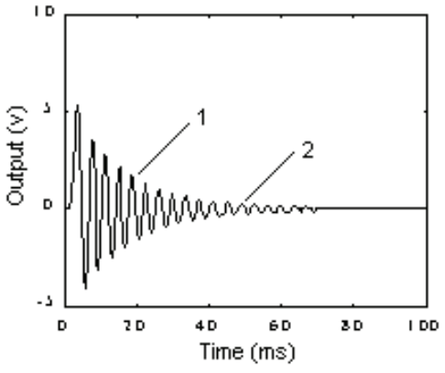

Fig. 6-6 Comparison of identification result and supposed response: (1) supposed response, and (2) identification result.

Parameter	a_1	a_2	b_0	b_1	b_2	c_1	c_2
Supposed	-1.95974	0.98681	0.00677	0.01353	0.00677	1.00	0.50
Identified	-1.95974	0.98681	0.00676	0.01350	0.00675	0.99995	0.50014

Table 6-2 Comparison between parameters supposed and identified

All above simulation results show that the performance and convergence of the algorithm presented in this section are good.

3. Modeling of wrist force sensor

The impulse response method is easily done and works well in the dynamic calibrations of sensors. So we adopt this method to make the dynamic calibration experiments of the wrist force sensor. In the calibration, a wrist force sensor is mounted on a testing platform. If no load is placed on the wrist sensor in the dynamic calibration, we call it no-load-calibration (NLC); while when there is some load laid on the wrist force sensor, we call it having-load-calibration (HLC). An impulse force is applied to the wrist force sensor with a hammer, that is, the hammer strikes vertically on the sensor directly in the NLC or on the load placed on the sensor in the HLC in a very short interval. In the head of the hammer, a piezoelectric sensor is installed to transform the impulse force into the electric charge signal. This signal is amplified by a charge amplifier and sent to a computer based data acquisition system. The wrist force sensor outputs six channel signals, of which three channels express force components of x, y, and z directions, and three channels express moment components of x, y, and z directions. These six channel signals of the wrist force sensor are also collected by the data acquisition system.

In the NLC, the zero point of work of the wrist force sensor is located in the middle part of the linear working range, so the dynamic response of the sensor is linear. But in HLC, the position of the zero point of work is moved from the linear working range to the nonlinear working range because of the applied load. Therefore the effect of the nonlinear factor becomes serious. The dynamic response of the sensor in HLC is nonlinear. The impulse response of NLC is shown in Fig. 6-7, and that of HLC in Fig. 6-8.

In order to demonstrate the superiority, in the modeling of sensors, of the algorithm presented in this section, the following work is done. First assume the models of sensors in NLC and HLC are linear, we carry out linear modeling (LM) using the LMS. Secondly we regard the models of sensors as nonlinear ones, and identify them with the algorithm presented in this section, which is nonlinear modeling (NLM). Finally we compare these identification results. Fig. 6-9 and Fig. 6-10 show their difference in terms of curves, and Table 6-3 and Table 6-4 in terms of parameters. The sum of square error $\sum e^2$ of each identified curve to the real impulse response is used to evaluate the accuracy of model, which is shown in Table 6-3 and Table 6-4. The smaller is the value of $\sum e^2$; the better is the identification result.

The two curves in Fig. 6-9 are almost overlapped to each other, and the identified parameters with the algorithm presented in this section contain a small coefficient value c_2 . It shows that the nonlinear factor of the impulse response in NLC is not very serious or there lies a quite weak non-linearity. But in Fig. 6-10, two curves have a little difference, and the value of coefficient c_2 is not a very small one. The nonlinear factor should be considered under this circumstance. Judging from the values of $\sum e^2$ in Table 6-3 and 6-4, we come to the conclusion that the nonlinear modeling method presented in this section is better than that of the linear modeling method in describing the model of the wrist force sensor.

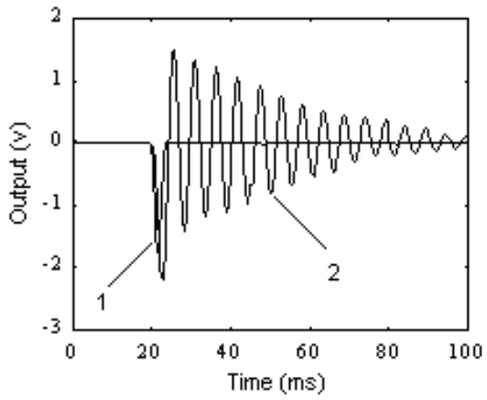

Fig. 6-7 Impulse response in NLC: (1) impulse input, and (2) dynamic response of the sensor.

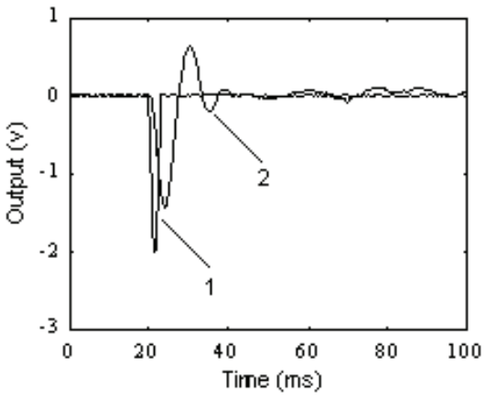

Fig. 6-8 Impulse response in HLC: (1) impulse input, and (2) dynamic response of the sensor.

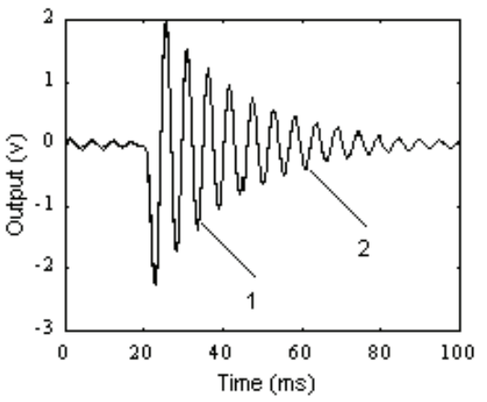

Fig. 6-9 Comparison of modeling in NLC with two kinds of methods: (1) modeling with LM, and (2) modeling with NLM.

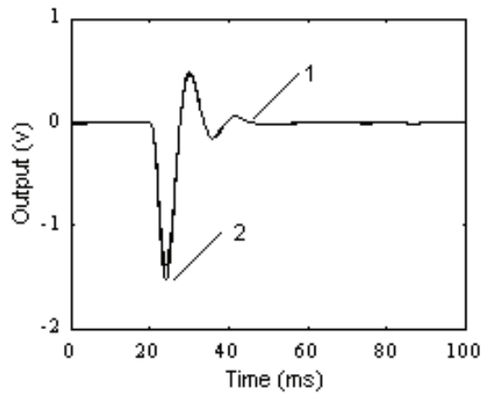

Fig. 6-10 Comparison of modeling in HLC with two kinds of methods: (1) modeling with LM, and (2) modeling with NLM.

Parameter	a_1	a_2	c_1	c_2	$\sum e^2$
LM	-1.97785	0.99095			15.97152
NLM	-1.97818	0.99138	0.89319	0.05800	12.08818

Table 6-3 Comparison between linear modeling and nonlinear modeling in NLC

Parameter	a_1	a_2	c_1	c_2	$\sum e^2$
LM	-1.96237	0.96528			3.45087
NLM	-1.96144	0.96438	1.48733	-0.19036	3.38959

Table 6-4 Comparison between linear modeling and nonlinear modeling in HLC

4. Discussions

The one-stage identification algorithm has advantages as follows: (1) One-stage identification simplifies the algorithm; (2) It depends only on the data of input and output of the system, not needing to introduce the auxiliary variables that could not be measured in practice; (3) It only needs dynamic calibration experimental data of systems, not needing to do static calibration experiments. On the basis of identification, the nonlinear dynamic compensation is easily completed.

6.2 Hammerstein model based correction

With the increasing higher requirement of the dynamic measurement, it is more and more important to improve the dynamic performances of sensors. We brought forward a nonlinear compensation method for the Hammerstein model. The Hammerstein model is composed of two parts, one linear dynamic unit and one nonlinear static subsystem, therefore the compensation includes two steps accordingly: The first step is linear dynamic compensation and the second one is nonlinear static correction. Thus we call it two-step compensation. Fig. 6-11 shows a block diagram of this method. The linear dynamic compensation unit is $h'(t)$, and the inverse unit of the nonlinear static subsystem $N(\cdot)$ is $N^{-1}(\cdot)$. The ultimate compensated output is $u'(t)$.

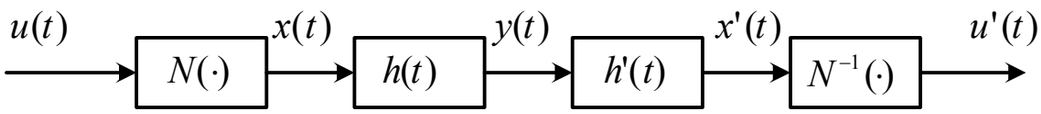

Fig. 6-11 A block diagram of two-step compensation

A linear dynamic compensation unit $h'(t)$ is designed using the pole-zero configuration method or system identification method [24]. Through the linear dynamic compensation, we get $x'(t)$. A nonlinear static correction unit $N^{-1}(\cdot)$ should be designed. The nonlinear static subsystem can be expressed by a second-degree polynomial.

$$N[u(k)] = x(k) = c_1 u(k) + c_2 u^2(k) \tag{6-20}$$

Its inverse system is assumed as

$$N^{-1}[\hat{x}(k)] = \hat{u}(k) = d_0 + d_1 \hat{x}(k) + d_2 \hat{x}^2(k) \tag{6-21}$$

Where $\hat{u}(k)$ and $\hat{x}(k)$ are the predictive data, $\hat{x}(k) = c_1 \hat{u}(k) + c_2 \hat{u}^2(k)$. Though c_1, c_2 have been obtained, $N^{-1}(\cdot)$ is still difficult to be solved from Equation (6-16). We adopt the FLANN to get the parameters d_0, d_1, d_2 of $N^{-1}(\cdot)$ as the artificial neural network has the excellent approximation property. A schematic diagram of the FLANN for training parameters is shown in Fig. 6-12.

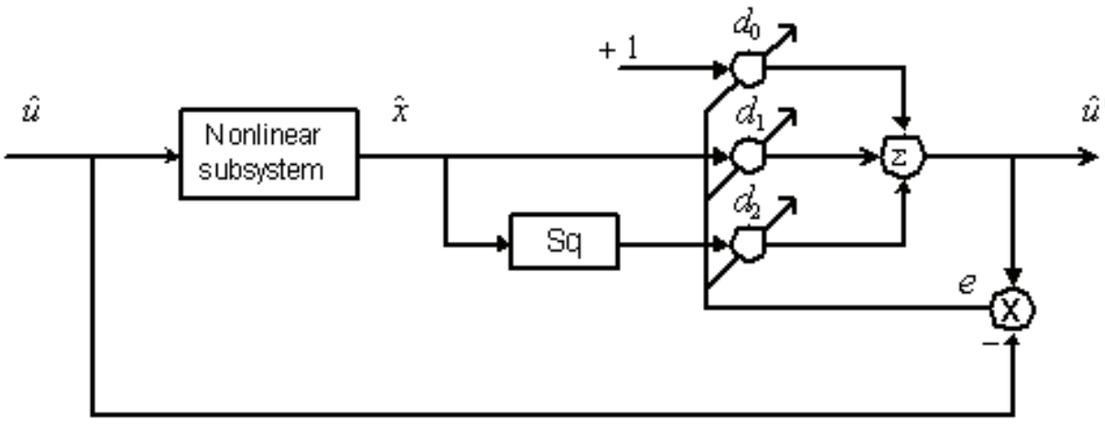

Fig. 6-12 A training schematic diagram of the FLANN

1. Simulations of nonlinear dynamic compensation

Using the compensation method stated above, the simulation results of the step response and impulse response are shown in Fig. 6-13 ~ Fig. 6-16. Fig. 6-13 and Fig. 6-15 show the results of the first step, that is linear dynamic compensation, compared with the output signal of sensors. Fig. 6-14 and Fig. 6-16 show the results of the second step, that is nonlinear static correction, compared with the input signal of sensors. It can be seen that the method of nonlinear dynamic compensation is effective.

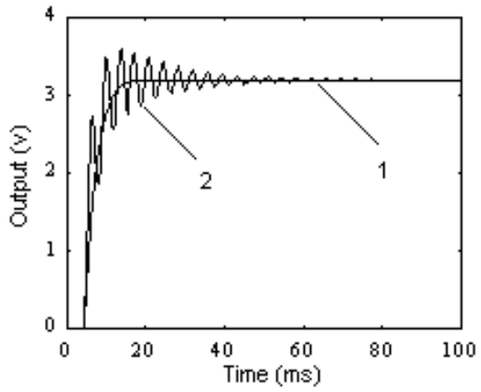

Fig. 6-13 The first step of compensation: (1) nonlinear dynamic response, and (2) dynamic compensation of the first step.

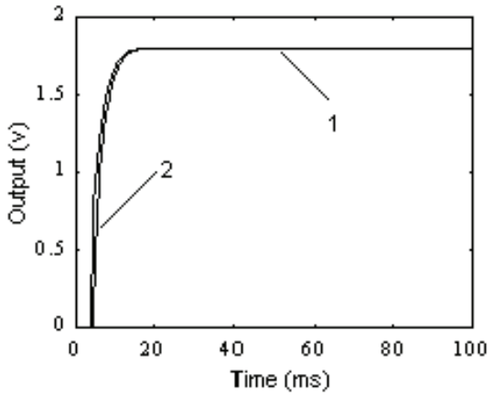

Fig. 6-14 The second step of compensation compared with the input signal (1) step input, (2) nonlinear static correction of the second step.

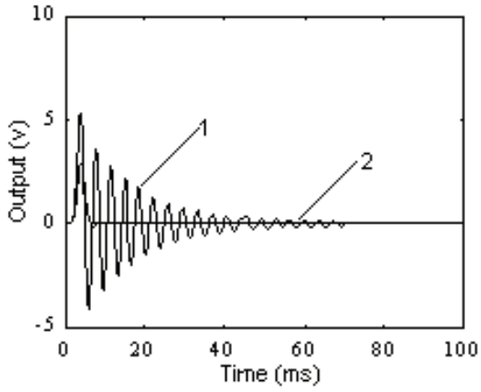

Fig. 6-15 The first step of compensation (1) nonlinear dynamic response, (2) dynamic compensation of the first step.

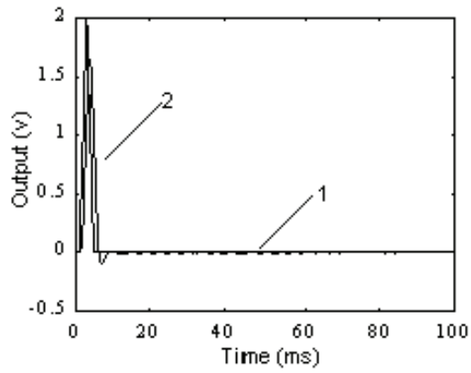

Fig. 6-16 The second step of compensation compared with the input signal (1) impulse input, (2) nonlinear static correction of the second step.

2. Compensation of the impulse response of wrist force sensor

The impulse responses of the wrist force sensors in NLC and HLC are compensated using the two-step nonlinear dynamic compensation method. Fig. 6-17 shows the result of the nonlinear dynamic compensation for NLC, and Fig. 6-18 shows the result of the linear dynamic compensation using the linear compensation method. Comparing the two results, we find that the compensation result in Fig. 6-17 is not better than that in Fig. 6-18, because the nonlinear dynamic factor is a weak one, as we have analyzed in above section.

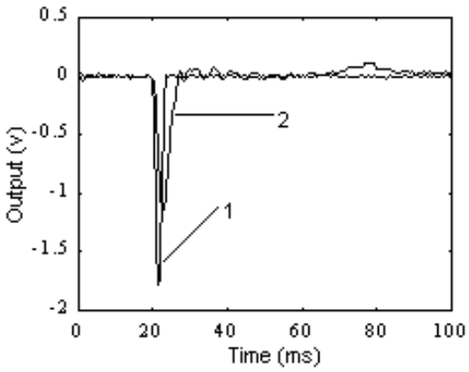

Fig. 6-17 Compensation result of NLC compared with the input signal (1) impulse input, (2) nonlinear dynamic compensation result

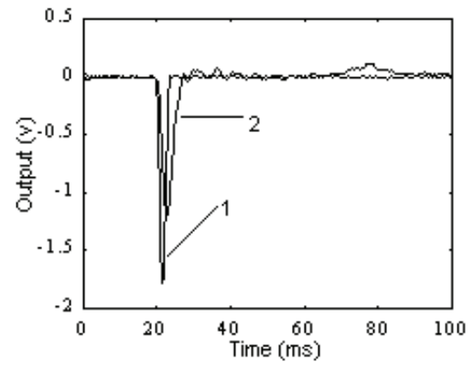

Fig. 6-18 Compensation result of NLC using linear approach compared with the input signal (1) impulse input, (2) compensation result

Fig. 6-19 shows the result of the nonlinear dynamic compensation for HLC, and Fig. 20 shows the result of the linear dynamic compensation for HLC. The nonlinear compensation method is better than the linear one in HLC.

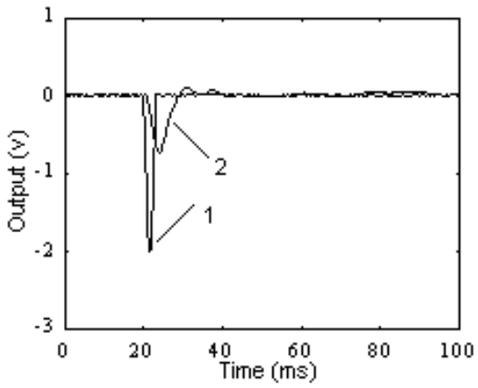

Fig. 6-19 Compensation result of HLC compared with input signal (1) impulse input, (2) nonlinear static correction of the second step

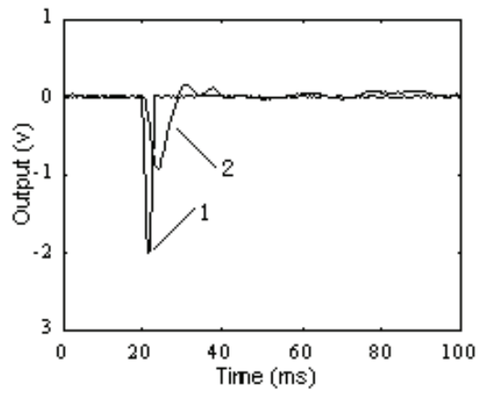

Fig. 6-20 Compensation result of HLC using linear approach compared with the input signal (1) impulse input, (2) compensation result

6.3 Wiener model based modeling and correction

A kind of nonlinear dynamic compensation method is proposed based on the Wiener model. Sensors with the nonlinear dynamic characteristics are describing as the Wiener model that is the cascade connection of a linear dynamic subsystem followed by a nonlinear static part. The nonlinear static characteristic of sensors is first corrected, and then the linear dynamic response is compensated. A DSP-based nonlinear dynamic compensating system and a sensor simulator are developed, and the experiments are carried out to demonstrate the effect of the nonlinear dynamic compensation method.

1. Principle of nonlinear dynamic compensation

Some sensors with the nonlinear dynamic characteristics can be divided into a linear dynamic subsystem and a nonlinear static part, which is shown in Fig. 6-21. They can be described by the differential equation as the following.

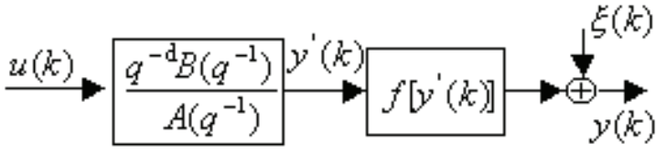

Fig. 6-21 Structure scheme of sensor after decomposition

$$\begin{cases} A(q^{-1})y'(k) = q^{-d}B(q^{-1})u(k) \\ y(k) = f[y'(k)] + \xi(k) \end{cases} \tag{6-22}$$

Where

$$A(q^{-1}) = 1 + a_1 q^{-1} + \cdots + a_n q^{-n}$$
$$B(q^{-1}) = b_0 + b_1 q^{-1} + \cdots + b_m q^{-m}$$

Where, $A(q^{-1})$ and $B(q^{-1})$ are polymerizations of n and m order, d is the time delay of the system, $f(\cdot)$ is the nonlinear static part, $y(k)$ and $u(k)$ are the output and input of the sensor, respectively, $\xi(k)$ is noise at the output end of the sensor, $y'(k)$ is the output of linear dynamic part, k is discrete time variable.

We design a nonlinear dynamic compensating system shown in Fig. 6-22. $G(s)$ is a transfer function of the linear dynamic subsystem of sensor, and y' is the output of the linear dynamic subsystem. $f(\cdot)$ expresses the nonlinear static relationship, which is monotonous, for examples,

$$y_i = c_0 + c_1 y_i' + c_2 (y_i')^2 + c_3 (y_i')^3 + \cdots, i = 0,1,\cdots,M \tag{6-23}$$

Where *i* is the amplitude variable.

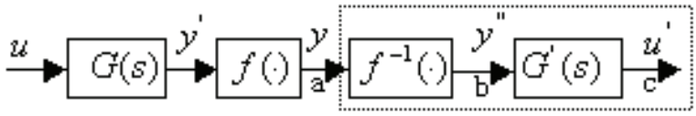

Fig. 6-22 Schematic diagram of sensor and compensating system

The frame that is dashed line shows the nonlinear dynamic compensating system. In the frame, $f^{-1}(\cdot)$ is the nonlinear static correcting part. After correction, the dynamic linear response $y''(k)$ is obtained. $G'(s)$ is the linear dynamic compensation part. After compensation, the output signal $u'(k)$ should express the measured signal $u(k)$ accurately.

2. Design of nonlinear dynamic compensation system

The design procedure of the nonlinear dynamic compensating system is given as follows.

a. Static calibration experiment

For example, a force sensor is load different weights in its measuring rang, and the sensor output are tested and recorded. Thus the sensor data of input and output $(y_i', y_i), i = 0,1,\cdots,M$, are collected, and the nonlinear static characteristic $f(\cdot)$ is obtained in Fig. 6-23.

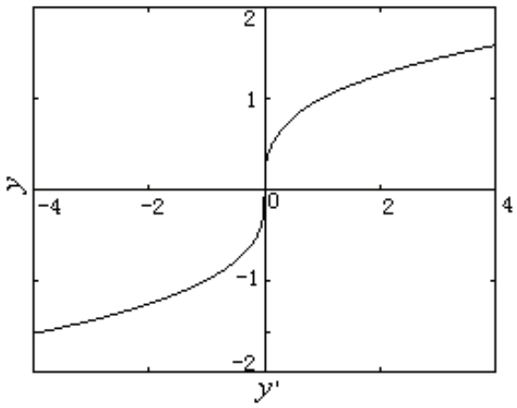

Fig. 6-23 Nonlinear curve

b. Design of nonlinear static correction subsystem

Assuming $f^{-1}(\cdot)$ is a reverse function of $f(\cdot)$. In some conditions, it is difficulty to obtain the reverse function $f^{-1}(\cdot)$. We adopt the method of looking up table. According to the nonlinear input and output of sensors, a table of correcting nonlinear is determined. In order to improve the precision of looking up table, the number of data in the table is increased using the interpolating method. Assuming the total number of data is $M+1$, the data in the table form are restored in the memory of a real time compensating system of the sensor, its distribution is shown in Fig. 6-24. The compensation system is connected with the sensor. The output signals of the sensor are firstly processed by the nonlinear static correction method. After correction, $y^{"} = y^{'}$, i.e. the nonlinear output become the linear output.

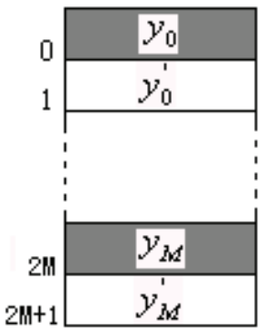

Fig. 6-24 Date distribution in the memory

c. Dynamic calibration experiment

For examples, the force sensor is applied to a negative step form force through sudden removing weights attaching to the sensor, and the sensor response is collected by a real time compensating system. The dynamic response acquired is linear because the compensation system has a function of correcting static non-linearity.

d. Design of linear dynamic compensation subsystem

According to the step input u of the sensor and the step response y' of the compensation system, a linear dynamic model in the form of differential equation is set up using the system identification or the artificial neural network. On the basis of the linear dynamic

model, a linear dynamic compensation subsystem can be designed using the pole-zero configuration method.

(1) The linear model of the sensor in the form of differential equation is transformed into the transfer function in the continuous domain.

(2) The zeroes of compensation part are designed as equal to the poles of linear dynamic part of the sensor. Thus the poles of sensor are canceled out completely or partly.

(3) According to the criterion that the damp ratio is 0.707 and natural frequency is not changeable, the poles of linear dynamic compensation subsystem are determined.

3. Development of nonlinear dynamic compensation system

The nonlinear dynamic compensating system is shown in Fig. 6-25. This system mainly includes an ADSP-2181 EZ-KIT Lite, an analog input part, an output part and the logic control circuit. The analog input part consists of eight sample and hold circuits (S/H), a multiplexer (MUX), an amplifier (AMP) and an analog to digital converter (A/D). The output part contains six digital to analog converters (D/A) and six RC filters. The logic control circuit mainly consists of a decoder. The ADSP-2181 EZ-KIT Lite is a minimal implementation of an ADSP-2181 processor designed by ADI Inc., and includes an ADSP-2181, an EPROM and a serial communication port et al. The outputs of sensors are connected to the inputs of S/Hs of the dynamic compensating system. It is controlled with the sampling frequency by ADSP-2181 that the sample mode is switched to the hold mode. The signals are switched and connected sequentially by MUX, amplified by the AMP, and sent to the A/D. A busy pin of A/D is connected to a programmable input/output pin. ADSP-2181 determines the reading time according to the state of busy pin.

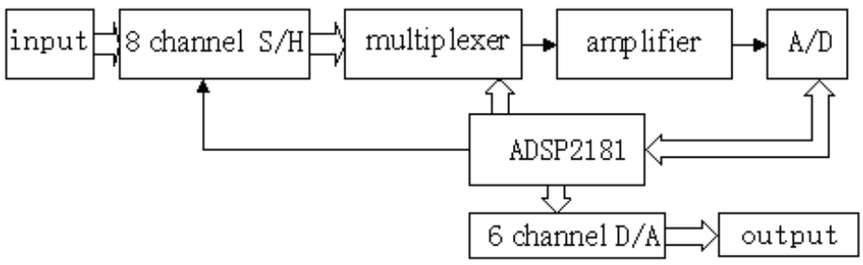

Fig. 6-25 Schematic block diagram of nonlinear dynamic compensating system

After multi-channel signals at the same time are acquired by ADSP-2181, they are processed by the nonlinear dynamic compensation method, and then are output by D/As. Under program control of ADSP-2181, the logic control circuit determines chip selects of A/D and D/A.

Software of the system includes data acquisition, data processing and result output. The sampling frequency of the system is determined by interrupt of timer, and is between $20\,K\ Hz\ \sim 25\,K\ Hz$. When power is applied to the system, the system start initialization, then enter the state of waiting for interruption. When the timer generates an interruption, the system begins a circle of data acquisition, processing and output.

4. Sensor simulator

In order to verify the effectiveness of nonlinear dynamic compensation method and system, a DSP-based simulating system of sensors is developed to produce the nonlinear dynamic

responses in various forms. The sensor simulator can also produce noise to exam the anti-disturbance of the nonlinear dynamic compensation system.

Fig. 6-26 shows the hardware schematic diagram of the sensor simulator. This system mainly includes an ADSP-2181 EZ-KIT Lite, an output part and logic control circuit. The output part contains eight digital to analog converters (D/A) and eight RC filters. The logic control circuit mainly consists of a decoder.

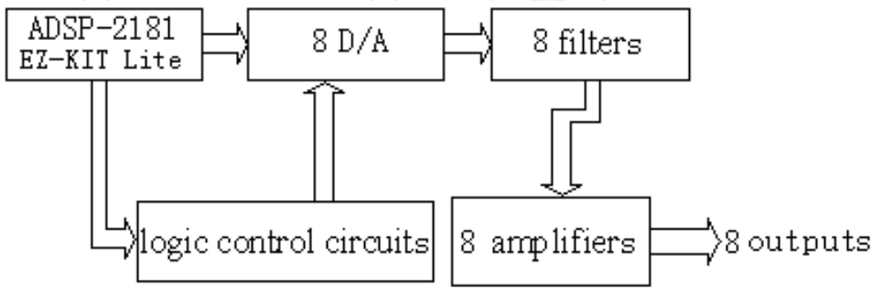

Fig. 6-26 Schematic block diagram of simulating system of sensors

The software flow chart of the sensor simulator is shown in Fig. 6-27. It includes an initialization, reading the input data, generation of the linear dynamic response by solving the differential equation, and generation of the nonlinear dynamic response through solving the nonlinear equation.

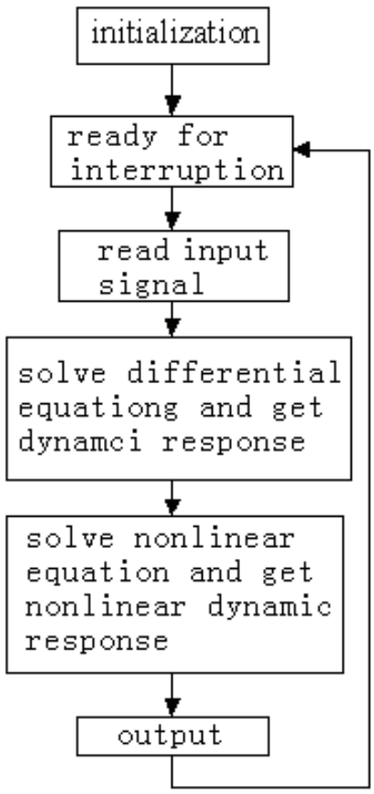

Fig. 6-27 Flow chart

5. Experiments

(1) Experimental setup

An experimental setup is shown in Fig. 6-28. PC1, PC2 and PC3 are personal computers. PC1 is in communication with the sensor simulator through a RS232. PC2 controls a scope through a GPIB to sample the outputs of the sensor simulator and compensating system. PC3 is connected with the compensating system through a RS232. The sensor simulator produces three channel signals as shown in Fig. 6-28. The channel 1 is the nonlinear output, the channel 2 is the linear output, and the channel 3 is the input signal. The compensating system has one input channel, i.e. the channel 4 that samples the nonlinear output of the sensor simulator. It has four output channels, the channel 5 is a direct output of sampled signal, the channel 6 is the nonlinear static correcting result, and the channel 7 is the dynamic compensating result.

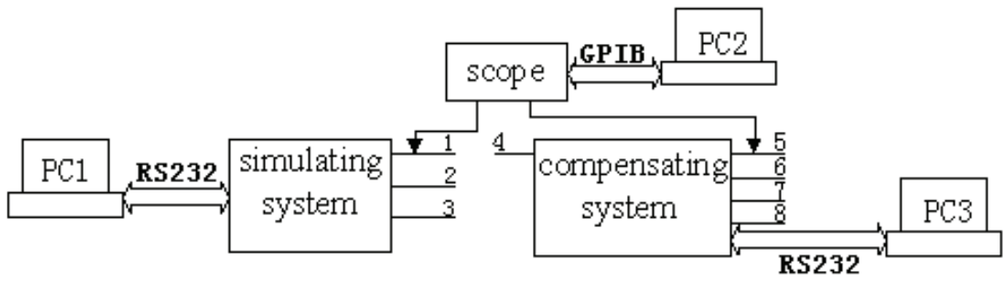

Fig. 6-28 Experimental setup

Assuming the linear part of the sensor is

$$y'(k) = 1.97097y'(k-1) - 0.99139y'(k-2) + 0.00527u(k) + 0.00233u(k-1) + 0.01282u(k-2) \quad (6\text{-}24)$$

The nonlinear part of the sensor is

$$y(k) = (y'(k))^{\frac{1}{3}} \quad (6\text{-}25)$$

(2) Nonlinear dynamic compensation process

The nonlinear dynamic compensating system is connected with the sensor simulator. It samples the output signal of the sensor. In one sampling interval, when one date is acquired, the corresponding linear output is obtained through the table of nonlinear correction, and then is handled using the linear dynamic compensation method.

(3) Experimental results

The step input and response of the sensor simulator are shown in Fig. 6-29. The result of nonlinear dynamic compensation, i.e. the output of the compensation system is shown in Fig. 6-30. The impulse input and response of the sensor simulator are shown in Fig. 6-31. The result of nonlinear dynamic compensation, i.e. the output of the compensation system is shown in Fig. 6-32. It is clear that the output of the compensation system is approximated to input of the sensor simulator, which proves that the nonlinear dynamic compensation method is effective.

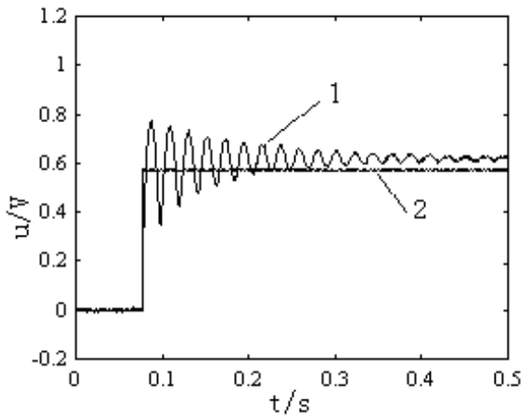

Fig. 6-29 Input and nonlinear output (1)nonlinear output, (2) input signal

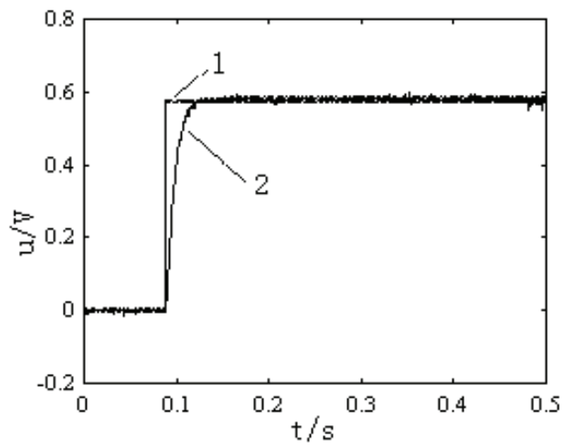

Fig. 6-30 Nonlinear output and compensating result (1) input signal, (2) compensated result

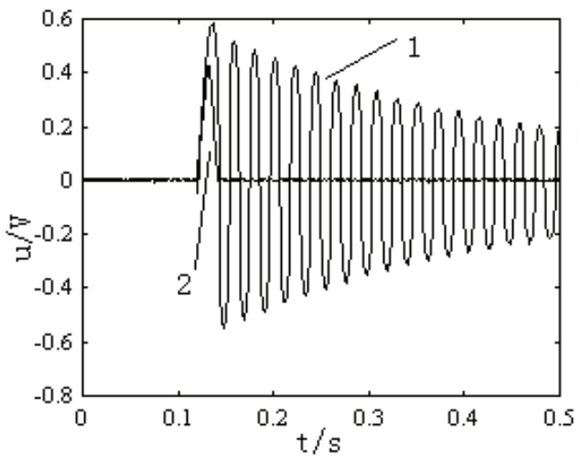

Fig. 6-32 Input and nonlinear output (1) nonlinear output, (2) input signal

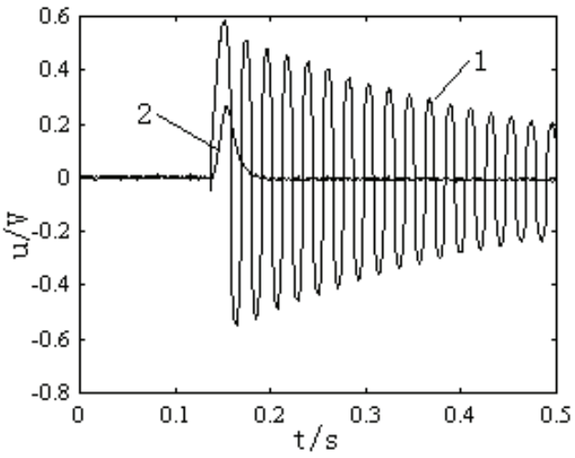

Fig. 6-33 Nonlinear output and compensation result (1) nonlinear output, (2) compensation result

6. Conclusions

(1) The dynamic response of sensors that posse the nonlinear dynamic characteristics is first handled using the nonlinear static correction method to obtain the linear dynamic response, and then is processed using the linear dynamic compensation method to short the time of reaching the steady state.

(2) This kind of method is applicable for different form and amplitude nonlinear dynamic responses of sensors.

(3) If there are noises in the nonlinear dynamic responses of sensors, a digital filter with two-order may be added into the compensation system. The place and order of the digital filter have been studied. The filter may be put the behind of the nonlinear static correction part or the linear dynamic compensation part. The cut-off frequency of the filter should be 2 times as large as the natural frequency of sensors.

7. References

Dwayne M. Perry, "Multi-axis force and torque sensing", Sensor Review, Vol.17, No.2, pp.117-120, 1997

Lu-Ping Chao,Kuen-tzong Chen , "Shape optimal design and force sensitivity evaluation of six-axis force sensors", Sensors and Actuators A, ol.63,pp. 105-112,1997

Maurice Dubious , "Six-component stain- gage balances for large wind tunnels", Experimental Mechanics, No.11, pp.401- 407,1981

Dirk Diddens, Dominiek Reynaerts , Hendrik Van Brussel , "Design of a ring- shaped three-axis micro force/torque sensor", Sensor and Actuators A , Vol.46-47,pp.225-232,1995

T. C. Hsia, "System Identification—Least Square Methods", Lexington Books, Lexington, Mass, 1977

P. Daponte et al. "Artificial neural networks in measurements", Measurement, Vol.23, No.2, pp.93-115,1998

J. C. Patra, G. Panda, R. Baliarsingh, "Artificial neural network-based non-linearity estimation of pressure sensors", IEEE Trans. Instru. Meas., Vol.63, No.6, pp.874-881, 1994

J. C. Patra, "An artificial neural network-based smart capacitive pressure sensor", Measurement, Vol.22, No.2, pp.113-121,1997

Ke-Jun Xu and Ting Tang, "A pole-zero offset method for sensor's dynamic compensation", Chinese Science Bulletin, Vol.39, No.16, pp.1407-1408, 1994

Ke-Jun Xu, Yin. Zhang and Chong-Wei Zhang , "Investigation of dynamic compensation for wrist force sensor", ACTA Metrologica Sinica, in Chinese, Vol.18, No.2,pp.116-121,1997

Waldemar Minkina, "Non-linear models of temperature sensor dynamics," Sensors & Actuators A, vol.30, pp.209-214, 1992

Waldemar Minkina, "Theoretical and experimental identification of the temperature sensor unit step response non-linearity during air temperature measurement," Sensors & Actuators A, vol.78, pp.81-87, 1999

Ping Wang, Shangshu Duan & Xinming Zhao et al, "Analysis the dynamic nonlinearity of transducers and its application in dynamic modeling," (in Chinese) Acta Metrologica Sinica, Vol.14, No.4, pp. 302-307, 1993

S. Beling, G. Blaeser, J. Bock, L. Heineit et al, "Signal conditioning for semiconductor gas sensors being used as detectors in gas-chromatographs and similar applications," Sensors & Actuators B, Vol.52, pp.15-22, 1998

Haixia Zhang & Hejun Li, "Nonlinear model of A^2PI^1 magnetic field sensor," Sensors & Actuators A, Vol.86, pp.206-210, 2000

Ke-Jun Xu and Cheng Li, "An estimation of nonlinear transfer function for wrist force sensor in frequency domain," (in Chinese) Journal of Applied Sciences, Vol.17, No.4, pp. 457-462,1999

Ke-Jun Xu and Cheng Li, "Dynamic nonlinear analysis of a wrist force sensor in the time and frequency domains," Proceedings of the 3rd World Congress on Intelligent Control and Automation, pp.1483-1487, Hefei, P. R. China, June 28 – July 2, 2000

Antonio Pardo, Santiago Marco, and Josep Samitier, "Nonlinear inverse dynamic models of gas sensing system based on chemical sensor arrays for quantitative measurements," IEEE Trans. on IM, vol.47, no.3, pp.644-651, 1998

Ke-Jun Xu, Zhi-Neng Zhu and Jia-Jun Liu, "Research on dynamic non-linearity compensation of sensor," (in Chinese) Proceedings of the 3rd World Congress on Intelligent Control and Automation, pp.1501-1504, Hefei, P. R. China, June 28 – July 2, 2000

Jozef Voros, "Iterative algorithm for parameter identification of Hammerstein systems with two-segment nonlinearities," IEEE Transactions on Automatic Control, Vol. 44, No.11, pp 2145-2149, 1999

Zhengliang Huang, Baiwu Wan and Chongzhao Han, "A two-stage identification technique for Hammerstein model," Control theory and applicatioon,Vol.12, No.1, pp.34-39, 1995

Ke-Jun Xu, "Applied research methods for dynamic characteristics of sensors," (in Chinese) Press of University of Science and Technology of China, 1999

Sensors: Focus on Tactile Force and Stress Sensors

Edited by Jose Gerardo Rocha and Senentxu Lanceros-Mendez

ISBN 978-953-7619-31-2
Hard cover, 444 pages
Publisher InTech
Published online 01, December, 2008
Published in print edition December, 2008

This book describes some devices that are commonly identified as tactile or force sensors. This is achieved with different degrees of detail, in a unique and actual resource, through the description of different approaches to this type of sensors. Understanding the design and the working principles of the sensors described here requires a multidisciplinary background of electrical engineering, mechanical engineering, physics, biology, etc. An attempt has been made to place side by side the most pertinent information in order to reach a more productive reading not only for professionals dedicated to the design of tactile sensors, but also for all other sensor users, as for example, in the field of robotics. The latest technologies presented in this book are more focused on information readout and processing: as new materials, micro and sub-micro sensors are available, wireless transmission and processing of the sensorial information, as well as some innovative methodologies for obtaining and interpreting tactile information are also strongly evolving.

How to reference

In order to correctly reference this scholarly work, feel free to copy and paste the following:

Ke-Jun Xu (2008). Study on Dynamic Characteristics of Six-Axis Wrist Force/Torque Sensor, Sensors: Focus on Tactile Force and Stress Sensors, Jose Gerardo Rocha and Senentxu Lanceros-Mendez (Ed.), ISBN: 978-953-7619-31-2, InTech, Available from: http://www.intechopen.com/books/sensors-focus-on-tactile-force-and-stress-sensors/study_on_dynamic_characteristics_of_six-axis_wrist_force_torque_sensor

INTECH
open science | open minds

InTech Europe
University Campus STeP Ri
Slavka Krautzeka 83/A
51000 Rijeka, Croatia
Phone: +385 (51) 770 447
Fax: +385 (51) 686 166
www.intechopen.com

InTech China
Unit 405, Office Block, Hotel Equatorial Shanghai
No.65, Yan An Road (West), Shanghai, 200040, China
中国上海市延安西路65号上海国际贵都大饭店办公楼405单元
Phone: +86-21-62489820
Fax: +86-21-62489821

IntechOpen